A panel of KSHV mutants in the polycistronic kaposin locus for precise analysis of individual protein products

Mariel Kleer[1,2,3], Grant MacNeil[4], Eric S. Pringle[4], and Jennifer A. Corcoran[1,2,3,4 #]

[1] Microbiology, Immunology and Infectious Diseases Department, University of Calgary, Calgary, AB, Canada.

[2]Charbonneau Cancer Institute, University of Calgary, Calgary, AB, Canada.

[3]Snyder Institute for Chronic Diseases, University of Calgary, Calgary, AB, Canada.

[4]Department of Microbiology and Immunology, Dalhousie University, Halifax, NS, Canada

[#]Corresponding Author

Abstract

Kaposi's sarcoma-associated herpesvirus (KSHV) is the cause of several human cancers including the endothelial cell (EC) malignancy, Kaposi's sarcoma. Unique KSHV genes absent from other human herpesvirus genomes, the "K-genes", are important for KSHV replication and pathogenesis. Among these, the kaposin transcript is highly expressed in all phases of infection, but its complex polycistronic nature has hindered functional analysis to date. At least three proteins are produced from the kaposin transcript: Kaposin A (KapA), B (KapB), and C (KapC). To determine the relative contributions of kaposin proteins during KSHV infection, we created a collection of mutant viruses unable to produce kaposin proteins individually or in combination. Kaposin-deficient latent iSLK cell lines displayed reduced viral genome copy number and often exhibited small LANA nuclear bodies; despite this, all were capable of progeny virion production. Primary infection with ΔKapB virus revealed decreased LANA expression and viral genome copy number, yet providing KapB protein *in trans* failed to complement these defects, suggesting a requirement for the *kaposin* locus *in cis*. Our previous work showed that KapB was sufficient to recapitulate the elevated proinflammatory cytokine transcripts associated with KS via the disassembly of RNA granules called processing bodies (PBs). We now show that KapB is necessary for PB disassembly during latent KSHV infection. These findings demonstrate that our panel of kaposin-deficient viruses enables precise analysis of the respective contributions of individual kaposin proteins to KSHV replication. Moreover, our mutagenesis approach serves as a guide for the functional analysis of other complex multicistronic viral loci.

Importance

Kaposi's sarcoma-associated herpesvirus (KSHV) expresses high levels of the kaposin transcript during both latent and lytic phases of replication. Due to its repetitive, GC-rich nature and

polycistronic coding capacity, until now no reagents existed to permit a methodical analysis of the role of individual kaposin proteins in KSHV replication. We report the creation of a panel of recombinant viruses and matched producer cell lines that delete kaposin proteins individually or in combination. We demonstrate the utility of this panel by confirming the requirement of one kaposin translation product to a key KSHV latency phenotype. This study describes a new panel of molecular tools for the KSHV field to enable precise analysis of the roles of individual kaposin proteins during KSHV infection.

44 **Introduction**

45 Kaposi's sarcoma-associated herpesvirus (KSHV) is the infectious cause of the
46 endothelial cell (EC) neoplasm, Kaposi's sarcoma (KS) and two rare lymphoproliferative
47 disorders: primary effusion lymphoma (PEL) and multicentric Castleman disease (MCD) (1–3).
48 Like all herpesviruses, KSHV establishes persistent, life-long infection of its human host, and
49 displays two modes of infection, latent and lytic replication. Latency is the default replication
50 program upon *de novo* infection in most cell types (4, 5). Following a transient period of lytic
51 gene expression which serves to amplify genome copy number and evade the intrinsic immune
52 response (6, 7), the viral episome is circularized and tethered to the host chromosome by the viral
53 latency-associated nuclear antigen (LANA) (8). This results in formation of microscopically
54 visible LANA-nuclear bodies (NB), which correlate with intracellular viral genome copy number
55 (9–13). In the latent state, the viral genome is passively replicated and unevenly partitioned to
56 daughter cells by host cell machinery (10, 14, 15). The viral genome will remain in a highly
57 chromatinized state until expression of the viral lytic switch protein, replication and transcription
58 activator (RTA), which is both necessary and sufficient for lytic reactivation (16–18). Following
59 reactivation, lytic gene expression follows a prescribed temporal cascade with genome
60 replication marking the transition from early to late gene expression (19, 20). More recent
61 analyses using single cell approaches show that lytic reactivation is quite heterogenous in terms
62 of viral gene expression, host cell responses and outcomes (13, 21–23). The lytic replication
63 phase produces progeny virions enabling transmission of the virus and culminates in cell death.

64 The KSHV-infected cells in KS lesions are predominantly proliferating endothelial cells
65 (ECs) with an abnormal elongated or 'spindled' morphology. The majority of these tumor ECs
66 exhibit latent KSHV infection, whereas lytic replication is limited (24–27). Lytic replication is

67 hypothesized to play a role in KS, likely due to the ongoing production of progeny virions as
68 well as the release of inflammatory and angiogenic factors (14, 28, 29). Consistent with this,
69 limiting viral lytic replication caused KS regression, suggesting that spontaneous lytic
70 reactivation is required for ongoing infection of naïve cells in the tumor environment and
71 supports the cancer (30–32).

72 As latently infected cells comprise the bulk of the KS lesion, the contribution of KSHV
73 latent gene expression to tumorigenesis has been explored extensively in both animal and cell
74 culture models (29, 33–37). *In vitro* infection of primary ECs with KSHV recapitulates many of
75 the features of KS tumors, including efficient establishment of viral latency. During latency,
76 gene expression is limited to six consensus protein products produced from an approximately
77 10kbp region of the viral genome termed the latency locus (LANA, viral cyclin [v-Cyclin], and
78 viral fas-associated death domain (FADD)-like interleukin-1-β-converting enzyme (FLICE)
79 inhibitory protein [v-FLIP], Kaposins [Kap] A, B, and C) and 12 pre-miRNAs that are processed
80 into at least 25 mature miRNAs (38–41) Using ectopic expression models, several latent gene
81 products have been shown to contribute to the establishment and maintenance of viral latency as
82 well as phenotypes associated with KS tumors (reviewed in (42, 43), but these studies have
83 predominantly focused on LANA, v-Cyclin and v-FLIP while the contributions of the
84 polycistronic kaposin locus is less clear. The kaposin mRNA was first identified as a marker of
85 KSHV latent infection in KS tumours in 1997 (27), and it remains the most abundant viral
86 transcript in KS tumor isolates (44). The kaposin locus comprises a significant fraction of KSHV
87 coding capacity during latency and kaposin transcription is also upregulated during lytic
88 replication, suggesting that this region of the viral genome is important (45). Despite this, we

89 still know very little about the role of the kaposin locus, or the proteins it encodes, during viral
90 replication.

91 The kaposin transcript is polycistronic and can be translated into at least three
92 polypeptides, KapA, KapB and KapC (Figure 1A) (45), though we and others have observed
93 multiple banding patterns on immunoblots that suggest additional translation products may also
94 be derived from this locus (45, 46). Translation of KapA is initiated at a canonical AUG start
95 codon located distal to the 5' end of the transcript and encodes a small membrane spanning
96 protein (47–49). KapC is translated in the same reading frame as KapA, making its carboxy-
97 terminal region identical to KapA. However, translation of KapC is initiated at one of two non-
98 canonical CUG start codons proximal to the 5' end of the transcript. Therefore, in addition to the
99 KapA ORF, the KapC translation product contains two 23-amino acid direct repeat (DR) regions
100 termed DR1 and DR2 (DR1: PSSPGTWCPPPREPGALLPGNLV and DR2:
101 APQEPGAAHPRNPARRTPGTRRG) which are derived from three sets of GC-rich 23-
102 nucleotide repeats (Figure 1A-B). Translation of KapB is initiated at one of two possible non-
103 canonical CUG or GUG start codons that are most proximal to the 5' end of the kaposin mRNA,
104 but uses an alternative reading frame to that of KapA/C. The resulting polypeptide is comprised
105 largely of the same two 23-amino acid DRs (DR1 and DR2) found in KapC (Figure 1B) but
106 lacks the C-terminal membrane spanning domain found in both KapA and KapC. Moreover,
107 different isolates of KSHV display expansion or contraction of both direct repeats, the functional
108 significance of which is unknown, yet regardless of the diversity in size, the core DR1 and DR2
109 repeats remain constant (45).

110 Our knowledge about individual kaposin protein function is derived largely from ectopic
111 expression of individual kaposin proteins. KapA was reported to promote cell transformation *in*

112 *vitro* and *in vivo* (47, 48); however, more recent work showed that this function stems from one
113 of the viral miRNAs embedded within the KapA ORF (50). Previous work from our group has
114 shown that KapB is sufficient to induce angiogenesis in an *in vitro* EC tubule formation assay
115 and to promote actin stress fibers and elongation of ECs into a spindled morphology that
116 recapitulates the morphology of latently infected KS tumor cells (51). KapB also is sufficient to
117 induce the disassembly of RNA granules called processing bodies (PBs) (51, 52). PBs are
118 important sites for the constitutive turnover or translational suppression of inflammatory
119 cytokine mRNAs; PB loss correlates with enhanced levels of inflammatory cytokine transcripts
120 that are normally targeted to PBs via an AU-rich destabilizing element (51, 53–57). However,
121 our previous studies could not determine if KapB alone is necessary for these phenotypes during
122 KSHV latent infection as we used RNA silencing to knockdown the kaposin transcript, a strategy
123 that reduced expression of all kaposin proteins (51). No other studies have determined the role of
124 individual kaposin translation products in KSHV latent or lytic replication cycles.

125 Here, we describe our use of the KSHV BAC16 bacterial artificial chromosome (BAC)
126 and lambda Red recombination system (58) to construct a panel of viruses defective for specific
127 *kaposin* locus products. We have constructed a triple deletion BAC16ΔKapABC, a double
128 deletion BAC16ΔKapBC, and two single deletions BAC16ΔKapB and BAC16ΔKapC (Figure
129 1C). We confirmed that these viruses no longer express the deleted kaposin-derived proteins and
130 show that all kaposin-deficient viruses are competent for genome replication and production of
131 progeny virions. However, we show that ΔKapB is significantly impaired, with markedly
132 reduced genome copy number, small LANA nuclear bodies, and lower LANA expression.
133 Moreover, these defects could not be complemented by providing KapB *in trans*. Additionally,
134 ΔKapB fails to cause PB disassembly following *de novo* infection of primary ECs, showing for

135 the first time that KapB is necessary for PB disassembly during KSHV latency. With this panel
136 of kaposin recombinant KSHV viruses, it is now feasible to interrogate, with unprecedented
137 precision, the role of individual kaposin protein products in the context of KSHV latent or lytic
138 infection.

139 **Materials and Methods:**

140 **Cell culture**

141 All cells were grown at 37°C with 5% CO_2 and atmospheric O_2. HEK293T cells (ATCC) were
142 cultured in DMEM (Thermo Fisher) supplemented with 100 U/mL penicillin, 100 µg/mL
143 streptomycin, 2 mM L-glutamine (Thermo Fisher) and 10% fetal bovine serum (FBS; Thermo
144 Fisher). iSLK.RTA cells (59) were cultured likewise with the addition of 1 µg/mL puromycin
145 and 250 µg/mL geneticin (Thermo Fisher). BAC16-iSLK.RTA cells were cultured similar to
146 iSLK.RTA cells, with the addition of 1200 µg/mL hygromycin B (Thermo Fisher). Human
147 umbilical vein endothelial cells (HUVECs, Lonza) were cultured in endothelial cell growth
148 medium (EGM-2) (Lonza). HUVECs were seeded onto gelatin (0.1% w/v in PBS)-coated tissue
149 culture plates or glass coverslips.

150 **Lambda Red recombination for BAC16 mutagenesis**

151 All mutagenesis was carried out in the BAC16 background (58) supplied in the GS1783 strain of
152 *Escherichia coli (E.coli)* (A generous gift from Dr. Jae Jung). All restriction enzymes were
153 purchased from New England Biolabs (NEB) and all primers were purchased from Invitrogen.

154 A kanamycin resistance and levansucrase enzyme cassette (KanSacB) was amplified using
155 primers (Table 1) with 40bp overhanging sequences that correspond to the K12 sequence of the
156 *kaposin* locus in the BAC16 genome. These primers also allowed for the introduction of BamHI
157 and NotI restriction endonuclease sites. The resulting PCR product was then subcloned into
158 pcDNA3.1+ (Addgene) using BamHI and NotI restriction endonucleases (pcDNA3.1+-
159 KanSacB).

160 To create single deletions of KapB and KapC, two direct repeat (DR) region gene blocks were
161 synthesized (BioBasic) where the third nucleotide of each codon of DR1 and DR2 was altered to
162 insert premature stop codons and nonsynonymous mutations into one frame, while creating
163 synonymous mutations in the other. This allowed the primary amino acid sequence of either
164 KapB or KapC to be maintained while eliminating expression from the other ORF and vice
165 versa. Primers were used to amplify the gene block with 40bp overhanging sequences that: 1)
166 flank the gene block, 2) are homologous to the upstream and downstream regions of the DRs in
167 the BAC16 genome, and 3) introduce NheI and BamHI restriction sites. The resulting PCR
168 product was then subcloned into pcDNA3.1+-KanSacB (described above) using NheI and
169 BamHI restriction sites (pcDNA3.1+-geneblock-KanSacB).

170 Lambda Red recombination was conducted in the GS1783 *E.coli* strain, which expresses
171 the I-Sce enzyme and, in a temperature (42°C) dependent manner, the lambda Red recombinase
172 genes (beta, exo and gam). BAC16-GS1783 *E. coli* were cultured at 30°C in Lysogeny Broth
173 (LB) containing 30 μg/mL chloramphenicol (Sigma-Aldrich) until reaching an optical density
174 (OD_{600}) of 0.6-0.8. Cultures were incubated for 30 minutes at 42°C prior to pelleting at room
175 temperature at 3000 x *g* for 5 minutes. Bacterial pellets were resuspended in ddH_20 and pelleted
176 again at 3000 x *g* for 5 minutes. This step was repeated once more, following which bacterial
177 pellets were resuspended in 50 μL ddH_20 and placed on ice. Meanwhile, pcDNA3.1+-geneblock-
178 KanSacB was digested with NheI and NotI restriction endonucleases to generate a linear DNA
179 fragment for recombination. This was purified by 1% agarose gel electrophoresis and gel
180 extracted according to QIAquick gel extraction kit (QIAGEN) standard protocol. The purified
181 fragment was electroporated (2.5kV, 25μF BioRad Gene Pulser®II) into 50 μL of ddH_2O-washed
182 BAC16-GS1783 *E.coli*. Bacteria was recovered for 1 hour in 1 mL of LB media at 30°C, plated

183 onto LB agar plates containing 50 µg/mL kanamycin, and incubated at 30°C overnight (O/N).
184 Colonies were screened for successful recombination using colony PCR and two sets of
185 screening primers designed to assess insert size and orientation (Table 1).

186 Colonies that produced bands of the expected size with both primer sets were inoculated
187 into 1 ml of LB containing 1% arabinose (Sigma-Aldrich) for 1 hour at 30°C to induce I-Sce
188 expression to linearize the inserted KanSacB cassette. Bacteria were then incubated at 42°C for
189 30 minutes to induce recombinase gene expression and recovered for 1 hour at 30°C prior to
190 plating on LB agar plates containing 30 μg/mL chloramphenicol and 5% sucrose, which selects
191 for the loss of SacB that synthesizes a toxic compound in the presence of sucrose. Positive
192 colonies were replica-plated on LB agar plates containing 50 µg/mL kanamycin. Those colonies
193 that grew on both chloramphenicol and sucrose containing plates, and which were no longer
194 kanamycin resistant, were screened by colony PCR for having undergone the second
195 recombination to remove the KanSacB cassette and colony PCR products were verified by
196 Sanger sequencing using primers as listed (Table 1).

197 **Isolation of BACmid DNA**

198 BACmid DNA was isolated from GS1783 *E.coli* cultures of 5 mL of LB containing 30 μg/mL
199 chloramphenicol grown O/N at 30°C. Bacteria was pelleted at 3000 x *g* for 5 minutes, re-
200 suspended in buffer P1 containing RNaseA, lysed using alkaline lysis in buffer P2 and
201 neutralized with buffer N3 (All reagents from QIAprep kits, QIAGEN). Following addition of
202 buffer N3, lysates were placed on ice for 10 minutes prior to centrifugation at 17 000 x *g* for 10
203 minutes to pellet precipitate. 750 µL of supernatant was then mixed with 750 µL of 100%
204 isopropanol and placed on ice for 10 minutes prior to centrifugation at 17 000 x *g* for 10 minutes

205 to pellet DNA. Supernatants were removed and the DNA pellet was left to air dry before being
206 resuspended in 50 µL 10mM Tris-Cl, pH 8.5. DNA was used immediately for transfection.

207 **Whole genome sequencing of KSHV BACs**

208 BACmid DNA was isolated from GS1783 *E.coli* cultures of 400 mL LB containing 30 μg/mL
209 chloramphenicol grown O/N at 30°C. Bacteria was pelleted at 4000 x *g* for 10 minutes at 4˚C.
210 DNA was then extracted using the Qiagen Large Construct Kit in accordance with
211 manufacturer's protocol. Critically, this isolation includes an exonuclease step which removes
212 sheared *E.coli* DNA thereby allowing greater coverage of the BAC16 genome.

213 Whole genome sequencing was performed by the Centre for Health Genomics and
214 Informatics (University of Calgary, Calgary, AB). Briefly, libraries were prepared using a NEB
215 ultra II DNA Library Prep Kit for Illumina (NEB), quantified using a Kapa qPCR Library Kit
216 (Roche), and sequenced using a MiSeq 500 v2 nano run (MiSeq Reagent Kit v2, Illumina) to
217 generate 250+250bp paired end sequences. Raw reads were imported into Geneious Prime (60),
218 paired and trimmed according to default settings. Reads were then aligned to the BAC16
219 reference genome (NCBI accession #GQ994935). Average coverage was between ~670 and
220 1400x. Variations were identified based on a minimum coverage of 5 and minimum frequency in
221 variation of 0.25.

222 **Restriction length fragment polymorphism**

223 Isolated BACmid DNA was digested overnight using NheI restriction enzyme (New England
224 Biolabs) at 37°C. Digested DNA fragments were then subjected to 1% agarose pulsed-field gel
225 electrophoresis (PFGE) (Bio-Rad) using 0.5% Tris/Borate/EDTA (TBE) buffer and the following
226 conditions: 6 V/cm, 120° field angle, and switch time linearly ramped from 1 s to 5 s over 14-15

227 h (CHEF DR III, Bio-Rad). DNA bands were visualized by staining the gel with a solution of 0.5
228 µg/mL ethidium bromide; excess stain was washed away with deionized water and the gel was
229 imaged on a ChemiDoc Touch Imaging System (Bio-Rad). DNA molecular weight standard
230 (BioRad, CHEF DNA size 8-48-kb) was used as reference.

231 **Generation of Stable BAC16-iSLK.RTA cell lines**

232 6-well plates of 70% confluent 293T cells in antibiotic-free 10% FBS DMEM were washed once
233 with PBS, and media was replaced with 1 mL serum-free, antibiotic-free DMEM per well prior
234 to transfection. 5 uL of re-suspended BAC16 DNA was incubated with 100 uL Opti-MEM
235 reduced serum media (Thermo Fisher) for 5 minutes. Separately, 18 uL of polyethylenimine
236 (PEI, Polysciences) was incubated with 100 uL Opti-MEM, also for 5 minutes. These two
237 mixtures were combined, incubated for 15 minutes, and added dropwise to each well. Cells were
238 incubated at 37°C for 4 hours at which time the media was replaced with antibiotic-free 10%
239 FBS DMEM before further incubation at 37C. This transfection procedure was used to create
240 latent 293T stable cell lines shown in Figure 3.

241 At 48 hours post transfection, cells were expanded into 10-cm dishes. One day later,
242 media was removed and replaced with fresh antibiotic-free 10% FBS DMEM containing 20
243 ug/mL hygromycin (Thermo Fisher Scientific). The concentration of hygromycin was steadily
244 increased until a final concentration of 100 μg/mL was reached. When a confluent monolayer of
245 hygromycin-resistant BAC16 293T cells was achieved, cells were split once prior to liquid N2
246 storage in 90% FBS and 10% dimethyl sulfoxide (DMSO, Sigma-Aldrich).

247 To generate latent iSLK cells, each population of BAC16-transfected 293T cells was
248 individually co-cultured with puromycin-resistant iSLK.RTA cells in a 6-well dish at a 2:1 ratio.

249 Once cells reached 80% confluency, media was replaced with antibiotic-free 10% FBS DMEM
250 containing 1 mM sodium butyrate (NaB, Sigma-Aldrich) and 20 ng/mL 12-O-
251 tetradecanoylphorbol-13-acetate (TPA, Sigma-Aldrich) to induce latent BAC16-293T cells to
252 produce progeny virions. At 96 hours post reactivation, cells were expanded into 10 cm dishes.
253 One day following expansion, media was replaced with antibiotic-free 10% FBS DMEM
254 containing 10 ug/mL puromycin and 100 μg/mL hygromycin. Hygromycin concentration was
255 steadily increased in approximately 50 μg/mL increments until a final concentration of 240
256 μg/mL was reached. Once a near-confluent monolayer of BAC16-iSLK.RTA cells was achieved,
257 cells were split once prior to liquid N_2 storage as above. This procedure was used to create the
258 latent iSLK cell lines shown in Figure 3. A single latent iSLK cell line was created for
259 ΔKapABC, ΔKapBC and ΔKapC, while we derived four latent iSLK cell lines for ΔKapB
260 independently, as shown in Figure 6.

261 **Production of KSHV BAC16 Wild-type and Recombinant Virus**

262 Each population of BAC16-iSLK cells were reactivated using 1 ug/mL Doxycycline (Dox,
263 Sigma-Aldrich) and 1 mM NaB in antibiotic-free 10% FBS DMEM. At 72 or 96 hours post
264 infection, supernatants were collected and clarified at 4000 x *g* to remove cellular debris and
265 virus-containing supernatant stored at -80°C prior to use.

266 ***De novo* infection of Naïve HEK293T of HUVEC cells**

267 Sub-confluent (50-70%) 12-well plates of 293T or HUVEC cells were incubated with viral
268 inoculum diluted in antibiotic and serum free DMEM containing 8 μg/mL hexadimethrine
269 bromide (polybrene; Sigma-Aldrich). Plates were centrifuged at 800 x *g* for 2 hours at room

270 temperature (61), the inoculum was removed and replaced with either antibiotic-free 10% FBS
271 DMEM (293T) or full EGM-2 (HUVECs). Cells were then returned to the 37°C incubator.

272 **Immunofluorescence**

273 Cells were seeded onto 18mm round (#1.5, Electron Microscopy Sciences) coverslips, infected
274 or treated as noted for each experiment and fixed for 10 minutes at room temperature in 4% (v/v)
275 paraformaldehyde (Electron Microscopy Sciences) in PBS. Samples were permeabilized with
276 0.1% (v/v) Triton X-100 (Sigma-Aldrich) in PBS for 10 min at room temperature and blocked in
277 1% human AB serum (Sigma-Aldrich) for 1 hour at room temperature. Primary antibody was
278 diluted in 1% human AB serum (Sigma-Aldrich) in PBS at the concentrations in Table 2 and
279 incubated overnight. The following day secondary antibody was likewise diluted in 1% human
280 AB serum, alongside Hoechst (ThermoFisher Scientific) for nuclear staining, at the
281 concentrations in Table 2 and incubated for one hour. Samples were mounted with Prolong Gold
282 AntiFade mounting media (ThermoFisher Scientific). Images were captured using a Zeiss
283 AxioObserver Z1 microscope with the 40X objective unless otherwise stated.

284 **Image analysis**

285 Image analysis was performed using CellProfiler (cellprofiler.org), an open source software for
286 image analysis (62). Quantification of hedls/EDC4 and LANA-nuclear body (NB) puncta was
287 performed as previously described (63) with the following modifications. Rather than staining
288 cells with wheat germ agglutinin to identify cell periphery, individual cell cytoplasms were
289 defined based on a 150-pixel propagation away from the Hoescht-stained nucleus. The number
290 of Hedls/EDC4 puncta within a defined cell cytoplasm was reported. To quantify the number of
291 puncta in KSHV-infected cells, a gating strategy was applied to include only cells with LANA-

292 positive nuclei and defined cell cytoplasms for Hedls/EDC4 puncta quantification. LANA-NBs
293 were defined by thresholding and size was measured using the "MeasureObjectSizeShape"
294 function, respectively. Object area refers to the number of pixels within the identified region. At
295 least 50 cells were quantified for each condition.

296 **Immunoblotting**

297 Cells were lysed in 1x Laemmli buffer (4% SDS, 20% glycerol, 120 mM Tris-Cl (pH 6.8) and
298 dd$H_2$0) and stored at -20°C until use. The DC Protein Assay (Bio-Rad) was used to quantify total
299 protein concentration as per the manufacturer's instructions. 10-15 µg of protein lysate was
300 resolved by SDS-PAGE on TGX Stain-Free acrylamide gels (BioRad). Membranes were blocked
301 in 5% BSA or 5% skim milk in Tris buffered saline-Tween20 (TBS-T). Primary and secondary
302 antibodies were diluted in 2.5% BSA or 2.5% skim milk, dilutions can be found in Table 1.
303 Membranes were visualized using ProtoGlow ECL (National Diagnostics) and the ChemiDoc
304 Touch Imaging system (BioRad).

305 **Intracellular viral genome qPCR**

306 Confluent 6-well plates of BAC16-iSLK.RTA cells were lysed using a DNeasy Blood and Tissue
307 Kit (Qiagen) according to manufacturer's protocol. Isolated DNA was stored at -20°C until
308 further use. DNA was diluted 1:30 prior to qPCR amplification using SsoFast EvaGreen
309 Supermix (Bio-Rad) and viral ORF26 or cellular β-actin (control) primers as listed in Table 3.
310 Fold change in viral genome copy number was determined using the ΔΔ-Quantitation cycle (Cq)
311 method.

312 **DNase-protected viral genome qPCR**

313 Supernatants from reactivated iSLK cells were harvested and clarified at 4000 x *g* for 5 minutes.
314 Aliquots of 180 µL were stored separately at -80°C prior to use. Supernatants were thawed at
315 37°C and mixed with 20 µL of a 500U DNaseI (NEB), 10X buffer and nuclease free water
316 mixture and incubated at 37°C for 30 minutes. DNA was then extracted using a DNeasy Blood
317 and Tissue Kit with the following adjustments: per sample, 500 µg of salmon sperm DNA
318 (Invitrogen) and 1 ng of a luciferase (*luc2*) containing plasmid (pGL4.26, Clontech) was added
319 to buffer AL prior to lysis. DNA was not diluted prior to qPCR amplification using SsoFast
320 EvaGreen Supermix (Bio-Rad) and viral ORF26 and *luc2* (control) primers as listed in Table 3.
321 Since every viral particle contains one genome, and one genome contains a single copy of the
322 ORF26 gene, the number of viral DNA molecules could be calculated. Fold change in viral
323 DNase-protected genomes was determined using the ΔΔ-Quantitation cycle (Cq) method.

324 **Lentivirus Production and Transduction**

325 All lentiviruses were generated using a second-generation system. Briefly, HEK293T cells were
326 transfected with pSPAX2, MD2G, and the plasmid containing a gene of interest using
327 polyethylenimine (PEI, Polysciences). psPAX2 was a gift from Didier Trono (Addgene plasmid
328 #12260) and pMD2.G was a gift from Didier Trono (Addgene plasmid #12259). Viral
329 supernatants were harvested 48 h post-transfection, clarified using a 0.45 µm polyethersulfone
330 filter (VWR), and frozen at -80°C until use. For transduction, lentiviruses were thawed at 37°C
331 and added to target cells in complete media containing 5 µg/mL polybrene (Sigma) for 24 h. The
332 media was changed to selection media containing 5 µg/mL blasticidin (Thermo) and cells were
333 selected for at least 48 h before proceeding with experiments.

334 **Transfection**

335 12-well plates of 70% confluent 293T cells in antibiotic-free 10% FBS DMEM were washed
336 once with PBS, and media was replaced with 1 mL serum-free, antibiotic-free DMEM per well
337 prior to transfection. Cells transfected with 1 µg of plasmids containing a gene of interest (Table
338 4) using polyethylenimine (PEI, Polysciences). 4 hours post transfection, media was replaced
339 with antibiotic-free 10% FBS DMEM.

340 **RT-qPCR**

341 RNA was collected using a RNeasy Plus Mini Kit (Qiagen) according to the manufacturer's
342 instructions and stored at -80°C until further use. RNA concentration was determined using a
343 NanoDrop One^{C} (Thermo) and 500 ng total was reverse transcribed using qScript XLT cDNA
344 SuperMix (QuantaBio) using a combination of random and oligo (dT) primers according to the
345 manufacturer's instructions. cDNA was diluted 1:10 for all RT-qPCR experiments and SsoFast
346 EvaGreen Mastermix (Biorad) was used to amplify cDNA. The ΔΔquantitation cycle (Cq)
347 method was used to determine the fold change in expression of target transcripts. qPCR primer
348 sequences can be found in Table 3.

349 **Statistics**

350 Data shown are the mean ± standard deviation (SD). Statistical significance was determined
351 using a paired Student's *t*-test. *P* values are indicated in figures, (*, $P < 0.05$; **, $P < 0.01$; ***,
352 $P < 0.001$; ****, $P < 0.0001$; ns, nonsignificant). All statistics were performed using GraphPad
353 Prism version 9.0.1.

354 **Data Availability**

355 All BAC16 virus sequences were deposited in the NCBI Sequence Read Archive (SRA) and are
356 accessible through the following SRA accession numbers: SAMN19671530 (WT KSHV

357 BAC16), SAMN19671876 (KSHV BAC16 ΔKapABC), SAMN19671877 (KSHV BAC16

358 ΔKapBC), SAMN19671902 (KSHV BAC16 ΔKapB), and SAMN19672118 (KSHV BAC16

359 ΔKapC).

360 **Results:**

361 **Construction of a panel of kaposin recombinant BAC16 KSHV viruses**

362 Work on the *kaposin* locus has been limited by the lack of recombinant viruses that target
363 this region. To address this limitation, we created a panel of recombinant viruses that delete
364 KapA, KapB and KapC individually or in combination. These recombinant viruses were created
365 using the KSHV bacterial artificial chromosome clone BAC16, which contains the pBelo45
366 plasmid inserted between the vIRF-1 and ORF57 genes of the JSC-1 KSHV isolate (58, 63). This
367 insertion encodes a red fluorescent protein (RFP) and a hygromycin resistance gene under the
368 control of a constitutive cellular promoter, to enable visual and chemical selection of BAC16-
369 containing cells, respectively. The wildtype (WT) kaposin mRNA encodes three open reading
370 frames (ORFs), KapA, KapB and KapC (Figure 1A). As a first step to create viruses that no
371 longer made one or more of these protein products, we removed the DR regions that encompass
372 the entire KapB ORF and most of the KapC ORF; in so doing, we created BAC16ΔKapBC. We
373 then mutated the KapA start codon in the context of BAC16ΔKapBC to create
374 BAC16ΔKapABC. However, creating single deletions of KapB and KapC by simple start codon
375 mutagenesis proved to be extremely difficult due to the GC-rich and repetitive nature of this
376 region. We decided to use an amino acid recoding strategy to construct BAC16 genomes that
377 failed to code for either KapB or KapC, but not both. While both ORFs are comprised largely of
378 23-nucleotide DRs that translate into 23-amino acid DRs, the ORFs are in different reading
379 frames. Using the BAC16 genome (accession #GQ994935), we designed two different gene
380 blocks with the nucleotide sequence of the DRs recoded. The first DNA construct was composed
381 of alternative codons that disrupted the protein coding capacity of the KapB ORF, due to several
382 nonsynonymous or nonsense mutations in the DRs, but contained only synonymous nucleotide

383 changes in the KapC ORF that did not disrupt its amino acid sequence (ΔKapB; Figure 1B). The
384 second gene block coded for the inverse mutant; DRs were re-coded such that the KapC ORF
385 contained nonsynonymous or nonsense mutations, while the KapB ORF contained synonymous
386 mutations that did not disrupt its amino acid sequence (ΔKapC; Figure 1B). This strategy also
387 drastically decreased the GC-content of DR region from 78% to 59.6% or 63.3% for ΔKapB and
388 ΔKapC, respectively, facilitating the Lambda Red-based recombination events that followed and
389 enabling us to use colony PCR screening during mutagenesis.

390 A two-step lambda Red-based recombination method in *E.coli* was used to facilitate
391 BAC16 mutagenesis (Fig 1C) as in (64). We isolated each recombinant BACmid from *E.coli* and
392 performed whole genome sequencing (WGS). Mapping of reads to the BAC16 reference genome
393 (NCBI accession #GQ994935) using Geneious Prime (60) revealed an average coverage per
394 nucleotide of between 670 and 1430x. Subsequent analysis of variants revealed that no off-
395 target mutations had occurred during recombination (Figure 2A). Few variants were observed
396 and these occurred within repetitive regions of the KSHV genome that also displayed low
397 coverage, as previously shown (65–67). Outside of these, the only other variants detected were
398 located in the region between the genes for vIRF-1 and ORF57 (Figure 2A). This is to be
399 expected, as this is where the pBelo45 plasmid was inserted to facilitate the creation of BAC16,
400 thereby altering the wild-type nucleotide sequence in this genomic location (58). We focused our
401 attention to the kaposin DRs in WT BAC16. The repetitive nature of this sequence makes it
402 difficult to resolve by WGS (68) and we observed low coverage. There was no coverage in the
403 DR region for both ΔKapABC and ΔKapBC constructs, consistent with the complete removal of
404 the DRs (Figure 2A). In contrast, we observed high read coverage of the recoded kaposin regions
405 in ΔKapB and ΔKapC viruses as recoding decreased the repetitive and GC-rich nature of the

406 DRs (Figure 2B, only WT and ΔKapB shown for simplicity). The consensus sequences produced
407 for these regions matched our recoded gene blocks, reaffirming successful recombination. Given
408 the difficulty in resolving DR regions through Illumina sequencing (68), we also checked the
409 BAC16 genomes using restriction fragment length polymorphism. BAC16 DNA isolated from
410 *E.coli* was digested using the restriction enzyme NheI, followed by pulse field gel
411 electrophoresis (PFGE) to resolve fragments. We observed fragment sizes consistent with
412 predictions from *in silico* analysis using NCBI accession #GQ994935 with the exception of the
413 fragment comprised largely of terminal repeats (TRs). We predicted that the TR-containing
414 fragment should migrate at 33 kbp; however, we did not observe a fragment of this size and
415 instead observed an unexpected fragment migrating at approximately 18 kbp. This suggested a
416 deletion of approximately 15 kbp, or 19 copies of the 801bp sequence, within this region. This
417 deletion has previously been observed in BAC16 (69) because the highly repetitive nature of the
418 TRs, as well as their high GC-content, renders them sensitive to recombination events (70, 71).
419 The smaller TR fragment was found in WT BAC16 and in all five recombinant viruses,
420 suggesting the event occurred prior to our mutagenesis, and that analysis of our panel kaposin-
421 deficient BAC16 viruses relative to WT would be unaffected. PFGE analysis also revealed a
422 second size discrepancy within the predicted kaposin-containing fragment which WGS was
423 unable to resolve due to the repetitive nature of the region. Based on *in silico* analysis, we
424 expected a 1200 bp fragment, yet the digestion of our WT BAC16 genome produced a 1000 bp
425 fragment. This suggests that over time the WT BAC16 construct lost 200bp, or approximately
426 three 23-amino acid repeats, within the DR region, making our recoded kaposin locus in ΔKapB
427 and ΔKapC viruses longer than the kaposin locus in WT BAC16. Because different KSHV
428 isolates possess variable numbers of repeats (45), it is not surprising to observe that this

429 repetitive genomic area experienced DR contraction during BAC16 DNA copying, like has been
430 observed for the *kaposin* locus in KSHV. In future studies, we hope to decipher whether there is
431 any functional significance to the number of each kaposin DR1 and DR2 for KSHV replication.

432 **Generation of stable BAC16-iSLK.RTA cell lines**

433 After sequencing, the BAC16 mutant genomes were used to generate stable iSLK cell
434 lines. A workhorse cell line for KSHV research, iSLK cells have been engineered to express the
435 viral lytic switch protein, RTA, in a Doxycycline (Dox)-inducible manner (59). These cells are
436 especially useful for KSHV research as they maintain tight control of latency and produce large
437 quantities of virus following the addition of Dox (59). However, iSLK cells were refractory to
438 transfection in our hands; thus, we first transfected BAC16 DNA into 293T cells to create stable
439 BAC16-293Ts for each BACmid (Figure 3A), as in (69). The efficiency of 293T transfection
440 was between 20-30%, as estimated by RFP expression. We gradually selected the transfected
441 cells with hygromycin until a confluent monolayer of RFP+ 293T cells was achieved (Figure
442 3B). Via quantitative PCR (qPCR) for viral DNA (ORF 26), we analyzed intracellular genome
443 copy number for each kaposin-deficient transfected 293T latent cell line and found that
444 intracellular genome copy number was similar to WT in each case (Figure 3C).

445 BAC16-containing 293T cells were then co-cultured with naïve iSLKs and reactivated
446 using a histone deacetylase inhibitor (NaB) and a protein kinase C agonist (TPA) to produce
447 progeny virions to enable primary infection of iSLKs (72–75). All kaposin-deficient viruses were
448 able to infect naïve iSLKs judging by RFP expression. The population of kaposin-deficient latent
449 iSLK cells for each recombinant was then expanded via gradual selection in the presence of
450 hygromycin to eliminate uninfected cells and puromycin to eliminate BAC16-293T cells, until a
451 confluent layer of RFP-positive cells was achieved (Figure 3D). Immediately after selection, we

452 analyzed the features of our iSLK latent cell lines. RFP-positive iSLKs cells were then stained by
453 immunofluorescence to visualize the viral latent protein LANA, which forms nuclear puncta
454 called LANA nuclear bodies (NBs) during KSHV infection (9–12) that were visible in all our
455 kaposin-deficient latent iSLK cell lines (Figure 3E), suggesting latency was successfully
456 established. We observed that not all LANA-positive cells were RFP-positive, a discrepancy that
457 has been reported by others (76). We also observed variable RFP intensity in our latent cell
458 populations and an overall decreased intensity of RFP signal in kaposin-deficient cell lines
459 relative to WT (Figure 3E). Using qPCR to quantify intracellular genome copy number of our
460 panel of latent iSLKs, we revealed that kaposin-deficient iSLKs contained 10-40% of the
461 genome copies observed in latent WT iSLKs (Figure 3F). These observations suggest the
462 possibility that KSHV recombinant viruses that lack the *kaposin* locus display defects in their
463 ability to establish latency and/or undergo genome amplification immediately following *de novo*
464 infection, a step that serves to increase latent episome copy number (6, 7).

465 Considering the possibility that *kaposin*-deficient KSHV recombinant viruses could be
466 less efficient at maintaining KSHV latency once already established, we decided to test how well
467 each latent cell population would maintain the viral genome compared to WT BAC16 latent
468 iSLKs in the absence of selective pressure. We passaged each latent cell line fifteen times in the
469 absence of hygromycin and determined intracellular genome copy number at each passage.
470 While WT BAC16 iSLKs displayed minimal episome loss over 15 passages (14, 77), we
471 observed that two of our kaposin-deficient recombinant viruses displayed accelerated genome
472 loss: ΔKapABC and ΔKapBC, whereas ΔKapB and ΔKapC genome copy number remained
473 steady over time (Figure 4A-B). Taken together with Figure 3, these data suggest that the

474 *kaposin* locus is important for the establishment of KSHV latency and may also contribute to its
475 maintenance.

476 **Cells latently infected with kaposin-deficient viruses produce progeny virions when**
477 **reactivated**

478 Having created latently infected iSLK cell lines for each of our recombinant viruses, we
479 first confirmed the absence of KapB and/or KapC protein products after 24 hours of reactivation
480 of our ΔKapABC, ΔKapBC, and ΔKapB/ΔKapC latent iSLK cell lines by immunoblotting with a
481 DR1-specific antibody (45) (Figure 5A). WT-infected cells exhibited a range of DR-specific
482 banding as has been previously observed, suggesting additional isoforms of KapB or KapC can
483 be translated (45, 46). Predominant bands at approximately 41kDa and 35kDa corresponded to
484 the predicted molecular weights of full-length KapC and KapB, respectively. As expected, due to
485 the absence of DR1 epitopes in these mutants, no KapB or KapC protein was detected in lysate
486 from reactivated ΔKapABC or ΔKapBC iSLKs. We observed a faint band was detected at
487 ~46kDa in lysate derived from ΔKapB-infected iSLKs which corresponds to the predicted
488 molecular weight of re-coded KapC (Figure 4A). This version of KapC is larger than that
489 encoded by our WT BAC16 because of the loss of DRs in our version of WT BAC16 (Figure 2).
490 A prominent band was consistently observed at ~42kDa in lysate from ΔKapC-infected iSLKs
491 which corresponds to the predicted molecular weight of re-coded KapB (Figure 5A), also larger
492 than WT-derived KapB for the same reason (Figure 2). We attempted to produce an anti-KapA
493 chicken yolk IgY antibody (78) using a customized antibody production service and an epitope
494 predicted to be immunodominant; however, the antibody failed to detect KapA in WT infection
495 or after ectopic expression and we did not use it further in these studies.

496 To determine if each of our kaposin-deficient iSLK cell lines was capable of reactivation,
497 completion of a full lytic replication cycle, and the production of progeny virions, we reactivated
498 the cell lines with Dox, to activate RTA expression, and NaB and measured intracellular genome
499 copy number by qPCR at 24, 48, 72, and 96 hours post reactivation. Genome copy number at
500 each time point was normalized to its matched starting genome copy number in latency since
501 each of the latent cell lines had a different episome copy number (Figure 3F) prior to
502 reactivation. For all recombinants, viral genome copy number significantly increased between 48
503 and 72 hours after reactivation (Figure 5B). WT and ΔKapB viruses exhibited ~15-fold increase
504 in intracellular genome copy number over latent copy number, ΔKapABC and ΔKapC viruses
505 demonstrated a ~40-fold increase, and ΔKapBC virus genome copy number increased ~200-fold
506 by 96 hours post reactivation. We then determined how the reactivation process altered viral
507 genome copy number for each kaposin-deficient recombinant relative to WT and observed that
508 all kaposin-deficient viruses except for ΔKapB reached the same relative genome copy number
509 as WT by 96 hours post reactivation despite starting with less genomes than WT (Figure 5C).
510 These data show that all kaposin-deficient viruses are capable of genome replication to increase
511 viral DNA copy number after reactivation. Because the starting point of the reactivation process
512 was unequal (WT latent iSLK cells have more viral episomes at the 'starting point' of
513 reactivation than any of the kaposin-deficient iSLK cell lines, including ΔKapBC latent iSLK
514 cells, Figure 3G), we were hesitant to draw quantitative conclusions about the efficiency of
515 genome replication after reactivation between our panel of kaposin-deficient viruses.

516 We next determined if kaposin-deficient reactivated iSLK cells released progeny virus
517 particles into the media. To do so, we harvested the virus-containing supernatant at 96 hours post
518 reactivation and subjected it to DNase digestion to eliminate unencapsidated viral DNA, then

519 extracted the capsid-protected DNA and conducted qPCR for viral DNA (Figure 5D). We found
520 that kaposin-deficient viruses released similar numbers of DNase-protected viral genomes to WT
521 (Figure 5D). Although this observation suggests that the ability to package genomic material,
522 assemble and release progeny virus does not require the *kaposin* locus, we and others have
523 observed that extracellular genome copy number does not always correlate with infectious virus
524 (21). To determine whether released virus from each kaposin-deficient latent iSLK cell line were
525 competent to infect naïve cells, we incubated a naïve monolayer of 293T cells with supernatant
526 from reactivated iSLK cells and 24 hours later, stained cells for the latent protein LANA. We
527 identified LANA-expressing cells in all 293T cell monolayers infected by the panel of kaposin-
528 deficient recombinant viruses, (Figure 5E) showing that each kaposin-deficient virus can produce
529 infectious progeny virions. This is consistent with our earlier observations using the 293T-iSLK
530 co-culture system, as this method of latent cell line creation relies on successful lytic replication
531 and virion production.

532 **Latent iSLK cells that lack Kaposin B display altered latency phenotypes**

533 Previous work from our lab used ectopic overexpression of KapB to characterize its
534 function independent of viral infection. Consequently, we were most interested in analyzing the
535 behaviour of the ΔKapB recombinant virus. We reactivated WT and ΔKapB-BAC16 iSLKs to
536 produce progeny virus, equalized extracellular genomic copy number, and infected naïve cells for
537 24 hours; however, we saw very few LANA-positive cells post infection (Figure 6A). Given the
538 inconsistencies between stable BAC16 cell lines reported by others (79, 80), we decided to re-
539 derive another ΔKapB-latent iSLK cell line. Using the same population of ΔKapB-BAC16-
540 transfected 293Ts cells and an identical protocol for co-culture, selection, and expansion, we
541 produced a new ΔKapB iSLK cell line that we will refer to as ΔKapB-2 iSLKs, whereas our

542 original ΔKapB iSLK cell line will be referred to as ΔKapB-1. Following ΔKapB-2 iSLK
543 reactivation, we noticed a greater cytopathic effect in reactivated ΔKapB-2 iSLKs than
544 previously observed in reactivated ΔKapB-1 iSLKs. We then equalized extracellular particle
545 number as above, infected naïve cells with ΔKapB-2 BAC16 and observed a 2-fold reduction in
546 LANA-positive cells compared to WT virus (Figure 6B), a great improvement compared to
547 ΔKapB-1. The large difference between infectious progeny production from ΔKapB-1 versus
548 ΔKapB-2 latent iSLKs prompted us to derive two additional ΔKapB iSLK cell lines as described
549 above, termed ΔKapB-3 and ΔKapB-4. We compared several features between these four
550 ΔKapB iSLK cell lines. We noted that although all four latent cell lines were RFP-positive,
551 ΔKapB-1 latent iSLK cells did not fluoresce as brightly as WT or the other ΔKapB latent cell
552 lines (Figure 6C). We stained these latent cells for LANA nuclear bodies (NBs) and observed
553 several differences between LANA NBs present in latent WT iSLKs compared to the four
554 ΔKapB latent iSLK cell lines (Figure 6D). Although WT latent cells had fewer LANA NBs per
555 cell than all four ΔKapB latent cell lines (Figure 6E), WT LANA NBs averaged a much larger
556 area than in ΔKapB latent cell lines (Figure 6F). Of the four ΔKapB latent cell lines, ΔKapB-4
557 displayed LANA NB character that most closely resembled WT; namely, fewer LANA NBs that
558 were brighter and larger (Figure 6D-F). However, all four ΔKapB latent cell lines showed
559 episome copy number ~10-25% that of WT latent iSLKs (Figure 6G). Of these, ΔKapB-2 and
560 ΔKapB-4 had the higher genome copy number, consistent with ΔKapB-2 iSLK improved
561 reactivation (ΔKapB-2, Figure 6B) and ΔKapB-4 iSLK LANA NB character (ΔKapB-4, Figure
562 6D-F). In addition, all four ΔKapB latent cell lines displayed reduced steady-state levels of
563 LANA protein compared to WT (Figure 6H). Taken together, these distinct differences clustered
564 the four ΔKapB iSLK latent cell lines as defective compared to WT in terms of key latency

565 phenotypes such as LANA NB area, steady-state levels of LANA protein, and KSHV genome
566 copy number.

567 To determine if we could restore the defects associated with LANA expression in the
568 established ΔKapB iSLK cell lines, we used lentiviruses to ectopically express KapB or an
569 empty vector control (Figure 7A-C). We used RT-qPCR to measure LANA transcript levels with
570 and without complementation. ΔKapB latent iSLK cell displayed ~10-40% of the LANA RNA
571 transcript levels detected in WT iSLKs (Figure 7A). Overexpression of KapB failed to alter
572 LANA transcript levels compared to the control in any of the ΔKapB iSLK cell lines (Figure
573 7B). Moreover, latent ΔKapB iSLK cell lines showed reduced steady-state levels of LANA
574 protein, as above, that was again not restored by providing KapB *in trans* (Figure 7C). To
575 determine if complementation with KapB prior to primary infection and latency establishment
576 could restore these defects, we transduced naïve iSLK cells with KapB-expressing or control
577 lentiviruses prior to primary infection with ΔKapB. KapB expression did not complement the
578 low genome copy number or reduced LANA protein level seen in ΔKapB-infected cells after
579 primary infection (Figure 7D-F). To test if KapB could complement primary infection of another
580 cell type, we transfected 293Ts with two different versions of KapB (KS lung and BAC16) prior
581 to primary infection. Neither version of KapB was able to rescue low KSHV genome copy
582 number or LANA protein levels after *de novo* infection of 293Ts (Figure 7G-I). Taken together,
583 these data suggest that an aspect of the kaposin locus is required *in cis,* as providing the KapB
584 polypeptide *in tran*s, via non-targeted lentiviral integration, cannot complement the defects
585 associated with ΔKapB latency after primary infection.

586 **KapB is required for processing body disassembly after *de novo* infection of HUVECs**

587 We have previously shown that ectopic expression of KapB in human umbilical vein
588 endothelial cells (HUVECs) is sufficient to recapitulate key phenotypes associated with KSHV
589 latency, including the disassembly of processing bodies (PBs), cytoplasmic RNA and protein
590 granules whose loss correlates with enhanced inflammatory cytokine RNAs (51, 53–57). To
591 determine if KapB was necessary for KSHV-induced PB loss, we reactivated ΔKapB-2 latent
592 iSLK cells and used this virus to infect HUVECs. After 96 hours post infection, we fixed the
593 infected cells and stained the monolayer for both LANA and for a PB-resident protein called
594 Hedls/EDC4 (81, 82). We observed that ~80-90% of the cell monolayer was infected with either
595 ΔKapB BAC16 or WT BAC16 virus. In LANA-positive cells that were infected with WT virus,
596 we observed a two-fold decrease in PBs per infected cell compared to the mock-infected control
597 (Figure 8A-B), as shown previously (51). In LANA-positive cells infected with ΔKapB-2 virus,
598 PB numbers were not significantly altered relative to the mock-infected control (Figure 8A-B).
599 We also confirmed that WT-infected HUVECs expressed KapB, but that KapB was absent in
600 ΔKapB-infected HUVECs (Figure 8C). These data reveal for the first time that the KapB protein
601 is not only sufficient but also necessary for KSHV-induced PB disassembly following *de novo*
602 infection.

603 PBs constitutively repress or degrade cytokine transcripts that contain AU-rich elements
604 (AREs); accordingly, we and others have observed that PB disassembly correlates with enhanced
605 steady-state levels of some cytokine transcripts (51, 53–57). After primary infection of HUVECs
606 with WT or ΔKapB, we measured steady-state levels of selected ARE-containing cytokine
607 transcripts by RT-qPCR (Figure 8D). We predicted that if PBs remain intact, as is after ΔKapB
608 infection, cytokine levels would be decreased relative WT-infected cells as the ARE-RNAs from
609 which they are expressed would be subject to PB-mediated decay. Consistent with this

610 hypothesis, after infection with ΔKapB, IL-6 transcript levels were much reduced relative to that
611 observed with WT infection (Figure 8D). This is the expected response for a cytokine mRNA
612 that is shuttled to PBs for constitutive decay. However, we did not observe a strong difference
613 between steady-state levels of other ARE-containing cytokine transcripts (VEGF, IL-1β, GM-
614 CSF) after WT versus ΔKapB infection (Figure 8D), as not all ARE-RNAs respond in the same
615 manner to altered PB dynamics, as shown in (83). Moreover, IL-6 mRNA levels are extremely
616 sensitive to changes in PBs (84) and we previously observed IL-6 transcript levels increase in
617 response PB disassembly induced by KapB (85). Taken together, these data show that KSHV-
618 induced PB disassembly correlates with ~2-3-fold increased steady-state level of the IL-6
619 transcript and that both PB disassembly and enhanced IL-6 RNA levels are absent in cells
620 infected with ΔKapB.

621 We previously showed that ectopic expression of KapB is sufficient to induce primary
622 ECs to elongate and spindle, thereby recapitulating the morphology of infected cells within KS
623 lesions (51, 86). However, others have observed that ectopic expression of v-FLIP likewise
624 elicits EC spindling (87) and that the deletion of v-FLIP from the viral genome eliminates EC
625 spindling, although this effect is overcome at high multiplicity of infection (88). To test if KapB
626 is necessary for EC spindling, we used WT of ΔKapB BAC16, derived as above, to infect
627 HUVECs, fixed cells at 96hpi and visualized spindling at low magnification by brightfield
628 microscopy or at high magnification by staining fixed cells with phalloidin to label actin
629 filaments. Robust cell spindling was observed in LANA-positive, WT-infected cells (Figure 9).
630 We also observed spindled cells in LANA-positive, ΔKapB-infected HUVECs (Figure 9). We
631 conclude that although ectopic expression of KapB is sufficient to elicit EC spindling (51), it is
632 not necessary for EC spindling during KSHV latency.

633 **Discussion:**

634 The kaposin locus comprises a significant portion of the coding capacity of the KSHV
635 latency locus, yet its role in KSHV latent and lytic replication is not fully appreciated. Prior to
636 this report, the KSHV field lacked recombinant viruses to enable functional analysis of
637 individual kaposin proteins in the context of KSHV infection. Here we described the
638 construction and validation of a suite of kaposin-deficient recombinant viruses using the BAC16
639 bacterial artificial chromosome and a panel of corresponding stable iSLK cell lines. We deleted
640 or recoded kaposin ORFs individually or in combination, generating several mutants: ΔKapABC,
641 ΔKapBC, ΔKapB, and ΔKapC. We showed that all kaposin-deficient viruses established latency
642 in iSLKs, replicated the viral genome upon reactivation, and produced progeny virions that could
643 be used for *de novo* infection of naïve cells. Despite this, all kaposin-deficient latent iSLK cells
644 lines displayed reduced viral genome copy number during latency compared to WT. In addition,
645 we characterized four derivations of ΔKapB-iSLKs and showed that these cells not only had
646 markedly reduced genome copy number, but also reduced LANA NB area and LANA RNA and
647 protein levels. Attempts to complement the reduced expression of LANA in ΔKapB-iSLKs by
648 ectopic expression of KapB had no effect, nor did attempts to complement the reduced KSHV
649 genome copy number after primary infection with ΔKapB virus. Together, these data suggest
650 that the kaposin locus plays a role in latency establishment that cannot be restored by
651 complementing with KapB protein *in trans*. Finally, we used ΔKapB BAC16 to show that KapB
652 is not only sufficient but also necessary for KSHV-mediated PB disassembly following *de novo*
653 infection of primary ECs, verifying the contribution of an individual kaposin protein to KSHV
654 biology. This toolkit will allow us to understand the role of the kaposin locus in KSHV
655 replication with unprecedented precision, making it a significant advance for the field.

656 Previous knowledge about the role of the kaposin locus was derived from studies using
657 the ectopic expression of individual kaposin ORFs (47, 51, 52, 89–91). To date, no
658 comprehensive kaposin-deficient BAC16 studies have been published. Toth *et al*., created a
659 kaposin knockout BAC16 virus by deleting a 1319-nucleotide region that included the coding
660 region of KapA and the majority of the coding regions of KapB and KapC (92). This
661 recombinant virus was used to test for the recruitment of proteins from polycomb repressive
662 complexes 1 and 2 to two lytic viral promoters after primary infection of SLK cells (92). For this
663 phenotype, the kaposin knockout virus displayed no difference from WT, but aside from this, no
664 additional analyses related to this mutant were reported. Gallo *et al.* created a K12 mutant in
665 which a kanamycin cassette disrupts the K12 ORF, but reported limited phenotypic analysis
666 related to this virus (93). Finally, Campbell *et al*. investigated the role of the RTA-responsive
667 element (RRE) promoter in the kaposin locus, and in so doing created a K12 RRE-mutant;
668 however, this study focused solely on RTA-recruitment and genomic architecture (94). In the
669 current study, our recombinant viruses were created by removing all DR1 and DR2 sequences
670 (ΔKapBC) with or without mutagenesis of the KapA ORF start codon (ΔKapABC), or by
671 replacing the DR region with alternatively coded nucleotide sequences (ΔKapB and ΔKapC).
672 Our recoding strategy had several advantages. First, the translation potential of the *kaposin* locus
673 was reduced by insertion of multiple termination codons, eliminating expression of some protein
674 products while maintaining other ORFs by alternative codon usage. Second, recoding destroyed
675 the repetitive nature of the locus and decreased the GC-content, making the region much more
676 amenable to error-free homologous recombination. Third, in all of the recombinant kaposin-
677 mutant BACs, regulatory sequences for transcription and miRNA processing were left intact. We
678 also created corresponding latent iSLK cell lines for the kaposin-deficient BAC16 constructs. All

679 four of these kaposin-deficient latent iSLK cell lines showed drastic reductions in viral genome
680 copy number compared to WT. The cell lines were created by co-culturing BAC16-transfected
681 HEK 293Ts with naïve iSLKs, a widely used method reported to be more efficient than direct
682 transfection of recombinant BAC16 DNA, that leverages cell-to-cell spread of virions from
683 reactivated 293T cells to iSLKs (5, 59, 69, 95). Despite using this strategy, we failed to produce
684 latent cell lines that contained high genome copy numbers for any of the kaposin-deficient
685 BAC16 DNA. We repeated the co-culture procedure for the most impaired of these four times,
686 and each attempt yielded similar results; all four ΔKapB iSLK cell lines displayed reduced viral
687 episome number and altered LANA NBs compared to WT BAC16 cells. Although these data are
688 consistent with the idea that kaposin-deficient viruses are impaired in one or more key steps
689 required for the establishment of latency, further study is required to characterize the nature of
690 this defect.

691 LANA expression and function is central to the establishment of KSHV latency. LANA
692 forms homo-oligomers and binds the terminal repeat (TR) regions of the KSHV genome while
693 simultaneously binding histones H2A and H2B of host chromatin, thereby tethering the viral
694 DNA to host chromosomes (8, 10, 11, 96). This binding leads to the formation of structures
695 called LANA NBs that colocalize with viral genomes (10, 97, 98). The number of LANA-
696 positive puncta in an infected cell correlates with the number of viral episomes (13). KSHV *de*
697 *novo* infection of a cell monolayer is heterogenous and results in variable levels of intracellular
698 viral genomes between individual latent cells, and this heterogeneity is also represented by
699 diverse LANA NB number per cell (13). Therefore, robust LANA NB staining is a marker for
700 successful latency establishment. We and others have observed heterogenous LANA NB size
701 within and between latent infected cells; however, the significance of this size variability is less

702 clear. Because LANA can bind to nucleosomes in cellular chromosomes as well as those bound
703 to viral episomes (15), LANA NBs are classified as supramolecular structures that cluster
704 multiple viral episomes together (12, 98). Genome clustering was proposed to be an effective
705 evolutionary strategy that allows KSHV to rapidly increase viral genome copy number per cell at
706 the expense of total number of cells infected (15). It is not yet clear if a minimum number of
707 viral episomes are required to create a supramolecular LANA NB after *de novo* infection;
708 however, WT KSHV does preferentially form clustered LANA NBs (15). We have observed that
709 latent ΔKapB iSLK cells possess smaller and more uniform LANA NBs compared to those
710 found in WT iSLK cells. Latent ΔKapB iSLK cells express lower amounts of LANA RNA and
711 protein, a phenotype that we could not complement by ectopic expression of KapB *in trans*.
712 Therefore, we report an additional correlative phenotype between low genome copy number,
713 lower LANA expression and smaller LANA NBs observed in multiple derivations of ΔKapB
714 latent iSLK cell lines and speculate that ΔKapB iSLK cells do not contain enough viral episomes
715 and/or LANA protein to form large LANA NBs with clustered genomes.

716 The kaposin locus overlaps with one of two possible viral origins of lytic genome
717 replication, called OriLytR. Though very few studies have investigated the contribution of
718 OriLytR/kaposin to viral genome replication, detailed analyses on the function of OriLytL have
719 revealed that it facilitates genome copying after viral reactivation and upon *de novo* infection
720 (99–102). More recent work has shown an essential role for OriLytL transcription in viral
721 genome replication after *de novo* infection (102). We speculate that loss of the GC-rich kaposin
722 repeat region in our mutants impairs the contribution of OriLytR to viral genome copying that
723 occurs after *de novo* infection, as was observed for a recombinant virus lacking OriLytL (102). A
724 reduction in viral genome copy number after *de novo* infection would be predicted to impair

725 latency establishment and diminish the clustering of viral episomes into larger LANA NBs,
726 which may explain the different LANA NB phenotype we observed in all four ΔKapB iSLK
727 latent cell lines. Since we failed to complement the low genome copy number observed after
728 primary infection with ΔKapB, these data suggest that the role of the *kaposin* locus after primary
729 infection is derived from either the DNA locus or its RNA transcript *in cis* and not from the
730 polypeptide provided *in trans*. At odds with our model is that the loss of the kaposin region does
731 not appear to negatively impact viral genome replication after reactivation. We speculate that this
732 step is not as sensitive to the loss of one of two functional origins of lytic replication, as also
733 observed for loss of OriLytL (120). Further experimentation will be needed to reveal the precise
734 mechanism by which kaposin region may promote genome amplification after primary infection
735 and how this alters LANA NB formation, function, and latency establishment.

736 KSHV latency predominates in most cells in culture and in KS tumours, suggesting viral
737 proteins expressed at this time are important in promoting tumourigenesis. We have previously
738 shown that ectopic expression of KapB in primary ECs recapitulates two features of the KS
739 lesion: cell spindling and elevated inflammatory cytokine expression via PB disassembly. Using
740 the ΔKapB BAC16 recombinant virus, we analyzed if KapB was not only sufficient but
741 necessary for these KSHV-associated tumor phenotypes. We show that after *de novo* infection of
742 HUVECs, ΔKapB BAC16 cells can induce cell spindling to a similar extent as WT BAC16
743 virus. These data are consistent with reports that the viral latent gene vFLIP is also capable of
744 causing endothelial cell spindling; therefore, the loss of KapB does not eliminate the spindling
745 phenotype (87). We propose that KapB and v-FLIP may act synergistically to promote EC
746 spindling during KSHV latency, and that in absence of one, the other is able to compensate. We
747 also used the ΔKapB BAC16 recombinant virus to determine if KapB was necessary for KSHV-

748 induced PB disassembly. PBs are cytoplasmic sites for the constitutive turnover or translational
749 suppression of ARE-containing inflammatory cytokine mRNAs (51, 53–57). We previously
750 showed that latent KSHV infection of primary ECs caused PB disassembly (51). Here, we also
751 observed that 96 hours after d*e novo* infection of HUVECs with WT BAC16, PBs were
752 disassembled. However, d*e novo* infection of HUVECs with ΔKapB BAC16 did not cause PB
753 disassembly, and steady-state levels of IL-6 RNA, an ARE-containing cytokine transcript known
754 to be regulated by PB levels, were reduced relative to that after WT infection (84). This reveals
755 that KapB is both necessary and sufficient for PB disassembly during KSHV latency and
756 represents the first time that a phenotypic function can be specifically attributed to a single
757 kaposin protein in the context of KSHV infection.

758 Our group and others showed that PBs also decrease during lytic replication and that
759 more than one viral protein is sufficient for this effect (53, 103). Here, we observed PB
760 disassembly 96 hours after *de novo* infection of HUVECs, and we have previously shown PB
761 disassembly in latent HUVECs (51). In contrast, Sharma *et al.* reported that PBs were not lost in
762 a KSHV-infected latent primary effusion lymphoma cell line. This discrepancy could be
763 attributed to the use of B-lymphocytes in their studies or their visualization of PBs by staining
764 largely for the PB-resident protein GW182, an antigen that has been shown to adopt a punctate
765 pattern distinct from other PB marker proteins (103, 104). Taken together, the observation that
766 KSHV encodes multiple proteins in both phases of its replication to elicit PB disassembly
767 suggests the functional relevance of this phenotype for viral infection. Because PBs
768 constitutively repress many pro-inflammatory, angiogenic, or pro-tumourigenic cellular
769 transcripts, we propose that the absence of microscopically visible PBs may contribute to the

770 inflammatory and angiogenic KS microenvironment and that KapB is necessary for this effect in
771 KS lesions.

772 In summary, this work describes the construction and preliminary analysis of four
773 different kaposin-deficient BAC16 viruses and corresponding iSLK latent cell lines. We used
774 these mutants to specifically attribute the phenotype of PB disassembly following *de novo*
775 infection of primary to the viral protein KapB. This work also provides preliminary data to
776 suggest that the *kaposin* locus aids in the establishment of KSHV latency after primary infection,
777 a role that may suggest that the region derives function from its GC-rich direct repeats in
778 addition to its protein products. This is exciting because it suggests that the *kaposin* locus is truly
779 multipurpose, deriving distinct functions important for viral replication from its RNA transcript,
780 and its protein products. We hope these mutants will enable future studies to better evaluate the
781 roles of individual kaposin protein products during infection. Moreover, we believe our strategy
782 to recode protein products in multiple reading frames can serve as a mutagenesis roadmap for
783 understanding other complex, polycistronic viral loci.

Acknowledgements

We sincerely thank the members of the Corcoran lab for helpful discussions about this work including Ms. Julie Ryu for designing recoded ΔKapB sequence. We would like to thank Dr. Craig McCormick (Dalhousie University) for valuable feedback on this manuscript and the McCormick lab for plasmids, expertise and advice. We would like to thank Dr. Anne Vaahtokari of the Charbonneau Microscopy Facility, UCalgary for microscopy support. We would like to thank Dr. John Archibald (Dalhousie University) and the Archibald lab for help performing pulse-field gel electrophoresis and Dr. Jae Jung (Cleveland Clinic) for sharing the BAC16-RFP bacterial artificial chromosome. MK was supported by a CSM graduate training award, a CIHR CGS-M scholarship, and a CIHR doctoral award. GM was supported by a CRTP graduate training award. Operating funds to support this work derive from a CIHR Project Grant PJT-153210 to JAC.

Author Contributions

Mariel Kleer: Conceptualization, Experimentation, Analysis, Paper Writing

Grant MacNeil: Conceptualization, Experimentation, Analysis

Eric S. Pringle: Conceptualization, Supervision

Jennifer A. Corcoran: Conceptualization, Experimentation, Supervision, Funding Acquisition, Project Administration, Paper Writing

Conflict of Interest

The authors have no competing interests to declare.

805 **References**

806 1. Chang Y, Cesarman E, Pessin MS, Lee F, Culpepper J, Knowles DM, Moore PS. 1994.
807 Identification of herpesvirus-like DNA sequences in AIDS-associated Kaposi's sarcoma.
808 Science (80-) https://doi.org/10.1126/science.7997879.

809 2. Cesarman E, Chang Y, Moore PS, Said JW, Knowles DM. 1995. Kaposi's sarcoma—
810 associated herpesvirus-like DNA sequences in AIDS-related body-cavity—based
811 lymphomas. N Engl J Med https://doi.org/10.1056/NEJM199505043321802.

812 3. Soulier J, Grollet L, Oksenhendler E, Cacoub P, Cazals-Hatem D, Babinet P, D'Agay MF,
813 Clauvel JP, Raphael M, Degos L, Sigaux F. 1995. Kaposi's sarcoma-associated
814 herpesvirus-like DNA sequences in multicentric Castleman's disease. Blood
815 https://doi.org/10.1182/blood.v86.4.1276.bloodjournal8641276.

816 4. Lagunoff M, Bechtel J, Venetsanakos E, Roy AM, Abbey N, Herndier B, Ganem D,
817 McMahon M, Ganem D. 2002. De Novo Infection and Serial Transmission of Kaposi ' s
818 Sarcoma-Associated Herpesvirus in Cultured Endothelial Cells. J Virol
819 https://doi.org/10.1128/JVI.76.5.2440.

820 5. Renne R, Blackbourn D, Whitby D, Levy J, Ganem D. 1998. Limited transmission of
821 Kaposi's sarcoma-associated herpesvirus in cultured cells. J Virol
822 https://doi.org/10.1128/JVI.72.6.5182-5188.1998.

823 6. Purushothaman P, Thakker S, Verma SC. 2015. Transcriptome Analysis of Kaposi's
824 Sarcoma-Associated Herpesvirus during De Novo Primary Infection of Human B and
825 Endothelial Cells . J Virol https://doi.org/10.1128/jvi.02507-14.

826 7. Krishnan HH, Naranatt PP, Smith MS, Zeng L, Bloomer C, Chandran B. 2004.
827 Concurrent Expression of Latent and a Limited Number of Lytic Genes with Immune
828 Modulation and Antiapoptotic Function by Kaposi's Sarcoma-Associated Herpesvirus
829 Early during Infection of Primary Endothelial and Fibroblast Cells and Subsequent
830 Decline of L. J Virol https://doi.org/10.1128/jvi.78.7.3601-3620.2004.

831 8. Cotter MA, Robertson ES. 1999. The latency-associated nuclear antigen tethers the
832 Kaposi's sarcoma- associated herpesvirus genome to host chromosomes in body cavity-
833 based lymphoma cells. Virology https://doi.org/10.1006/viro.1999.9999.

834 9. Szekely L, Kiss C, Mattsson K, Kashuba E, Pokrovskaja K, Juhasz A, Holmvall P, Klein
835 G. 1999. Human herpesvirus-8-encoded LNA-1 accumulates in heterochromatin-
836 associated nuclear bodies. J Gen Virol https://doi.org/10.1099/0022-1317-80-11-2889.

837 10. Ballestas ME, Chatis PA, Kaye KM. 1999. Efficient persistence of extrachromosomal
838 KSHV DNA mediated by latency- associated nuclear antigen. Science (80-)
839 https://doi.org/10.1126/science.284.5414.641.

840 11. Schwam DR, Luciano RL, Mahajan SS, Wong L, Wilson AC. 2000. Carboxy Terminus of
841 Human Herpesvirus 8 Latency-Associated Nuclear Antigen Mediates Dimerization,
842 Transcriptional Repression, and Targeting to Nuclear Bodies. J Virol
843 https://doi.org/10.1128/jvi.74.18.8532-8540.2000.

844 12. De Leo A, Deng Z, Vladimirova O, Chen HS, Dheekollu J, Calderon A, Myers KA,
845 Hayden J, Keeney F, Kaufer BB, Yuan Y, Robertson E, Lieberman PM. 2019. LANA
846 oligomeric architecture is essential for KSHV nuclear body formation and viral genome
847 maintenance during latency. PLoS Pathog https://doi.org/10.1371/journal.ppat.1007489.

848 13. Adang LA, Parsons CH, Kedes DH. 2006. Asynchronous Progression through the Lytic
849 Cascade and Variations in Intracellular Viral Loads Revealed by High-Throughput Single-
850 Cell Analysis of Kaposi's Sarcoma-Associated Herpesvirus Infection. J Virol
851 https://doi.org/10.1128/jvi.01156-06.

852 14. Grundhoff A, Ganem D. 2004. Inefficient establishment of KSHV latency suggests an
853 additional role for continued lytic replication in Kaposi sarcoma pathogenesis. J Clin
854 Invest https://doi.org/10.1172/JCI200417803.

855 15. Chiu YF, Sugden AU, Fox K, Hayes M, Sugden B. 2017. Kaposi's sarcoma-associated
856 herpesvirus stably clusters its genomes across generations to maintain itself
857 extrachromosomally. J Cell Biol https://doi.org/10.1083/jcb.201702013.

858 16. Lukac DM, Renne R, Kirshner JR, Ganem D. 1998. Reactivation of Kaposi's sarcoma-
859 associated herpesvirus infection from latency by expression of the ORF 50 transactivator,
860 a homolog of the EBV R protein. Virology https://doi.org/10.1006/viro.1998.9486.

861 17. Lukac DM, Kirshner JR, Ganem D. 1999. Transcriptional Activation by the Product of
862 Open Reading Frame 50 of Kaposi's Sarcoma-Associated Herpesvirus Is Required for
863 Lytic Viral Reactivation in B Cells. J Virol https://doi.org/10.1128/jvi.73.11.9348-
864 9361.1999.

865 18. Xu Y, AuCoin DP, Huete AR, Cei SA, Hanson LJ, Pari GS. 2005. A Kaposi's Sarcoma-
866 Associated Herpesvirus/Human Herpesvirus 8 ORF50 Deletion Mutant Is Defective for
867 Reactivation of Latent Virus and DNA Replication. J Virol
868 https://doi.org/10.1128/jvi.79.6.3479-3487.2005.

869 19. Sun R, Lin S-F, Staskus K, Gradoville L, Grogan E, Haase A, Miller G. 1999. Kinetics of

870 Kaposi's Sarcoma-Associated Herpesvirus Gene Expression. J Virol
871 https://doi.org/10.1128/jvi.73.3.2232-2242.1999.

872 20. Sun R, Lin SF, Gradoville L, Yuan Y, Zhu F, Miller G. 1998. A viral gene that activates
873 lytic cycle expression of Kaposi's sarcoma-associated herpesvirus. Proc Natl Acad Sci U
874 S A https://doi.org/10.1073/pnas.95.18.10866.

875 21. Nakajima K, Guevara-Plunkett S, Chuang F, Wang K-H, Lyu Y, Kumar A, Luxardi G,
876 Izumiya C, Soulika A, Campbell M, Izumiya Y. 2020. Rainbow Kaposi's Sarcoma-
877 Associated Herpesvirus Revealed Heterogenic Replication with Dynamic Gene
878 Expression. J Virol https://doi.org/10.1128/jvi.01565-19.

879 22. Chen CP, Lyu Y, Chuang F, Nakano K, Izumiya C, Jin D, Campbell M, Izumiya Y. 2017.
880 Kaposi's Sarcoma-Associated Herpesvirus Hijacks RNA Polymerase II To Create a Viral
881 Transcriptional Factory. J Virol https://doi.org/10.1128/jvi.02491-16.

882 23. Okoid LM, Kimballid AK, Kasparid RE, Knoxid AN, Coleman CB, Rochford R, Chang
883 T, Alderete B, van Dyk LF, Clambey ET. 2019. Multidimensional analysis of
884 gammaherpesvirus RNA expression reveals unexpected heterogeneity of gene expression.
885 PLoS Pathog https://doi.org/10.1371/journal.ppat.1007849.

886 24. Zhong W, Wang H, Herndier B, Ganem D. 1996. Restricted expression of Kaposi
887 sarcoma-associated herpesvirus (human herpesvirus 8) genes in Kaposi sarcoma. Proc
888 Natl Acad Sci U S A https://doi.org/10.1073/pnas.93.13.6641.

889 25. Katano H, Sato Y, Kurata T, Mori S, Sata T. 2000. Expression and localization of human
890 herpesvirus 8-encoded proteins in primary effusion lymphoma, Kaposi's sarcoma, and
891 multicentric Castleman's disease. Virology https://doi.org/10.1006/viro.2000.0196.

892 26. Katano H, Sato Y, Itoh H, Sata T. 2001. Expression of human herpesvirus 8 (HHV-8)-
893 encoded immediate early protein, open reading frame 50, in HHV-8-associated diseases. J
894 Hum Virol.

895 27. Staskus KA, Gebhard K, Haase AT, Zhong W, Wang H, Renne R, Ganem D, Herndier B,
896 Beneke J, Pudney J, Anderson DJ. 1997. Kaposi's sarcoma-associated herpesvirus gene
897 expression in endothelial (spindle) tumor cells. J Virol.

898 28. Bais C, Santomasso B, Coso O, Arvanitakis L, Raaka EG, Gutkind JS, Asch AS,
899 Cesarman E, Gerhengorn MC, Mesri EA. 1998. G-protein-coupled receptor of Kaposi's
900 sarcoma-associated herpesvirus is a viral oncogene and angiogenesis activator. Nature
901 https://doi.org/10.1038/34193.

902 29. Montaner S, Sodhi A, Molinolo A, Bugge TH, Sawai ET, He Y, Li Y, Ray PE, Gutkind
903 JS. 2003. Endothelial infection with KSHV genes in vivo reveals that vGPCR initiates
904 Kaposi's sarcomagenesis and can promote the tumorigenic potential of viral latent genes.
905 Cancer Cell https://doi.org/10.1016/S1535-6108(02)00237-4.

906 30. Mazzi R, Parisi SG, Sarmati L, Uccella I, Nicastri E, Carolo G, Gatti F, Concia E,
907 Andreoni M. 2001. Efficacy of cidofovir on human herpesvirus 8 viraemia and Kaposi's
908 sarcoma progression in two patients with AIDS [1]. AIDS.

909 31. Mesri EA, Feitelson MA, Munger K. 2014. Human viral oncogenesis: A cancer hallmarks
910 analysis. Cell Host Microbe.

911 32. Martin DF, Kuppermann BD, Wolitz RA, Palestine AG, Li H, Robinson CA. 1999. Oral
912 Ganciclovir for Patients with Cytomegalovirus Retinitis Treated with a Ganciclovir
913 Implant. N Engl J Med https://doi.org/10.1056/nejm199904083401402.

914 33. Bravo Cruz AG, Damania B. 2019. In Vivo Models of Oncoproteins Encoded by
915 Kaposi's Sarcoma-Associated Herpesvirus . J Virol https://doi.org/10.1128/jvi.01053-18.

916 34. Friborg J, Kong WP, Hottlger MO, Nabel GJ. 1999. p53 Inhibition by the LANA protein
917 of KSHV protects against cell death. Nature https://doi.org/10.1038/47266.

918 35. Fujimuro M, Wu FY, Aprhys C, Kajumbula H, Young DB, Hayward GS, Hayward SD.
919 2003. A novel viral mechanism for dysregulation of β-catenin in Kaposi's sarcoma-
920 associated herpesvirus latency. Nat Med https://doi.org/10.1038/nm829.

921 36. Radkov SA, Kellam P, Boshoff C. 2000. The latent nuclear antigen of Kaposi sarcoma-
922 associated herpesvirus targets the retinoblastoma-E2F pathway and with the oncogene
923 Hras transforms primary rat cells. Nat Med https://doi.org/10.1038/80459.

924 37. Sin SH, Dittmer DP. 2013. Viral latency locus augments B-cell response in vivo to induce
925 chronic marginal zone enlargement, plasma cell hyperplasia, and lymphoma. Blood
926 https://doi.org/10.1182/blood-2012-03-415620.

927 38. Qin J, Li W, Gao SJ, Lu C. 2017. KSHV microRNAs: Tricks of the Devil. Trends
928 Microbiol.

929 39. Arias C, Weisburd B, Stern-Ginossar N, Mercier A, Madrid AS, Bellare P, Holdorf M,
930 Weissman JS, Ganem D. 2014. KSHV 2.0: A Comprehensive Annotation of the Kaposi's
931 Sarcoma-Associated Herpesvirus Genome Using Next-Generation Sequencing Reveals
932 Novel Genomic and Functional Features. PLoS Pathog
933 https://doi.org/10.1371/journal.ppat.1003847.

934 40. Sarid R, Flore O, Bohenzky RA, Chang Y, Moore PS. 1998. Transcription Mapping of the

935 Kaposi's Sarcoma-Associated Herpesvirus (Human Herpesvirus 8) Genome in a Body
936 Cavity-Based Lymphoma Cell Line (BC-1). J Virol https://doi.org/10.1128/jvi.72.2.1005-
937 1012.1998.

938 41. Dittmer D, Lagunoff M, Renne R, Staskus K, Haase A, Ganem D. 1998. A Cluster of
939 Latently Expressed Genes in Kaposi's Sarcoma-Associated Herpesvirus. J Virol
940 https://doi.org/10.1128/jvi.72.10.8309-8315.1998.

941 42. Schulz TF, Cesarman E. 2015. Kaposi Sarcoma-associated Herpesvirus: Mechanisms of
942 oncogenesis. Curr Opin Virol.

943 43. Dittmer DP, Damania B. 2016. Kaposi sarcoma-associated herpesvirus: Immunobiology,
944 oncogenesis, and therapy. J Clin Invest.

945 44. Rose TM, Bruce AG, Barcy S, Fitzgibbon M, Matsumoto LR, Ikoma M, Casper C, Orem
946 J, Phipps W. 2018. Quantitative RNAseq analysis of Ugandan KS tumors reveals KSHV
947 gene expression dominated by transcription from the LTd downstream latency promoter.
948 PLoS Pathog https://doi.org/10.1371/journal.ppat.1007441.

949 45. Sadler R, Wu L, Forghani B, Renne R, Zhong W, Herndier B, Ganem D. 1999. A complex
950 translational program generates multiple novel proteins from the latently expressed
951 kaposin (K12) locus of Kaposi's sarcoma-associated herpesvirus. J Virol.

952 46. McCormick C, Ganem D. 2006. Phosphorylation and Function of the Kaposin B Direct
953 Repeats of Kaposi's Sarcoma-Associated Herpesvirus. J Virol
954 https://doi.org/10.1128/jvi.02331-05.

955 47. Kliche S, Nagel W, Kremmer E, Atzler C, Ege A, Knorr T, Koszinowski U, Kolanus W,

956 Haas J. 2001. Signaling by human herpesvirus 8 kaposin a through direct membrane
957 recruitment of cytohesin-1. Mol Cell https://doi.org/10.1016/S1097-2765(01)00227-1.

958 48. Muralidhar S, Pumfery AM, Hassani M, Sadaie MR, Kishishita M, Brady JN, Doniger J,
959 Medveczky P, Rosenthal LJ. 1998. Identification of kaposin (open reading frame K12) as
960 a human herpesvirus 8 (Kaposi's sarcoma-associated herpesvirus) transforming gene. J
961 Virol.

962 49. Tomkowicz B, Singh SP, Cartas M, Srinivasan A. 2002. Human herpesvirus-8 encoded
963 kaposin: Subcellular localization using immunofluorescence and biochemical approaches.
964 DNA Cell Biol https://doi.org/10.1089/10445490252925413.

965 50. Forte E, Raja AN, Shamulailatpam P, Manzano M, Schipma MJ, Casey JL, Gottwein E.
966 2015. MicroRNA-Mediated Transformation by the Kaposi's Sarcoma-Associated
967 Herpesvirus Kaposin Locus. J Virol https://doi.org/10.1128/jvi.03317-14.

968 51. Corcoran JA, Johnston BP, McCormick C. 2015. Viral Activation of MK2-hsp27-
969 p115RhoGEF-RhoA Signaling Axis Causes Cytoskeletal Rearrangements, P-body
970 Disruption and ARE-mRNA Stabilization. PLoS Pathog
971 https://doi.org/10.1371/journal.ppat.1004597.

972 52. McCormick C, Ganem D. 2005. The kaposin B protein of KSHV activates the p38/MK2
973 pathway and stabilizes cytokine mRNAs. Science (80-)
974 https://doi.org/10.1126/science.1105779.

975 53. Corcoran JA, Khaperskyy DA, Johnston BP, King CA, Cyr DP, Olsthoorn A V.,
976 McCormick C. 2012. Kaposi's Sarcoma-Associated Herpesvirus G-Protein-Coupled
977 Receptor Prevents AU-Rich-Element-Mediated mRNA Decay. J Virol

978 https://doi.org/10.1128/jvi.00597-12.

979 54. Blanco FF, Sanduja S, Deane NG, Blackshear PJ, Dixon DA. 2014. Transforming Growth
980 Factor Regulates P-Body Formation through Induction of the mRNA Decay Factor
981 Tristetraprolin. Mol Cell Biol https://doi.org/10.1128/mcb.01020-13.

982 55. Franks TM, Lykke-Andersen J. 2007. TTP and BRF proteins nucleate processing body
983 formation to silence mRNAs with AU-rich elements. Genes Dev
984 https://doi.org/10.1101/gad.1494707.

985 56. Vindry C, Marnef A, Broomhead H, Twyffels L, Ozgur S, Stoecklin G, Llorian M, Smith
986 CW, Mata J, Weil D, Standart N. 2017. Dual RNA Processing Roles of Pat1b via
987 Cytoplasmic Lsm1-7 and Nuclear Lsm2-8 Complexes. Cell Rep
988 https://doi.org/10.1016/j.celrep.2017.06.091.

989 57. Hubstenberger A, Courel M, Bénard M, Souquere S, Ernoult-Lange M, Chouaib R, Yi Z,
990 Morlot JB, Munier A, Fradet M, Daunesse M, Bertrand E, Pierron G, Mozziconacci J,
991 Kress M, Weil D. 2017. P-Body Purification Reveals the Condensation of Repressed
992 mRNA Regulons. Mol Cell https://doi.org/10.1016/j.molcel.2017.09.003.

993 58. Brulois KF, Chang H, Lee AS-Y, Ensser A, Wong L-Y, Toth Z, Lee SH, Lee H-R,
994 Myoung J, Ganem D, Oh T-K, Kim JF, Gao S-J, Jung JU. 2012. Construction and
995 Manipulation of a New Kaposi's Sarcoma-Associated Herpesvirus Bacterial Artificial
996 Chromosome Clone. J Virol https://doi.org/10.1128/jvi.01019-12.

997 59. Myoung J, Ganem D. 2011. Generation of a doxycycline-inducible KSHV producer cell
998 line of endothelial origin: Maintenance of tight latency with efficient reactivation upon
999 induction. J Virol Methods https://doi.org/10.1016/j.jviromet.2011.03.012.

1000 60. Kearse M, Moir R, Wilson A, Stones-Havas S, Cheung M, Sturrock S, Buxton S, Cooper
1001 A, Markowitz S, Duran C, Thierer T, Ashton B, Meintjes P, Drummond A. 2012.
1002 Geneious Basic: An integrated and extendable desktop software platform for the
1003 organization and analysis of sequence data. Bioinformatics
1004 https://doi.org/10.1093/bioinformatics/bts199.

1005 61. Yoo SM, Ahn AK, Seo T, Hong HB, Chung MA, Jung SD, Cho H, Lee MS. 2008.
1006 Centrifugal enhancement of Kaposi's sarcoma-associated virus infection of human
1007 endothelial cells in vitro. J Virol Methods https://doi.org/10.1016/j.jviromet.2008.07.026.

1008 62. Carpenter AE, Jones TR, Lamprecht MR, Clarke C, Kang IH, Friman O, Guertin DA,
1009 Chang JH, Lindquist RA, Moffat J, Golland P, Sabatini DM. 2006. CellProfiler: Image
1010 analysis software for identifying and quantifying cell phenotypes. Genome Biol
1011 https://doi.org/10.1186/gb-2006-7-10-r100.

1012 63. Cannon JS, Ciufo D, Hawkins AL, Griffin CA, Borowitz MJ, Hayward GS, Ambinder RF.
1013 2000. A New Primary Effusion Lymphoma-Derived Cell Line Yields a Highly Infectious
1014 Kaposi's Sarcoma Herpesvirus-Containing Supernatant. J Virol
1015 https://doi.org/10.1128/jvi.74.21.10187-10193.2000.

1016 64. Tischer BK, Von Einem J, Kaufer B, Osterrieder N. 2006. Two-step Red-mediated
1017 recombination for versatile high-efficiency markerless DNA manipulation in Escherichia
1018 coli. Biotechniques https://doi.org/10.2144/000112096.

1019 65. Santiago JC, Goldman JD, Zhao H, Pankow AP, Okuku F, Schmitt MW, Chen LH, Hill
1020 CA, Casper C, Phipps WT, Mullins JI. 2021. Intra-host changes in Kaposi sarcoma-
1021 associated herpesvirus genomes in Ugandan adults with Kaposi sarcoma. PLoS Pathog

1022 https://doi.org/10.1371/journal.ppat.1008594.

1023 66. BeltCappellino A, Majerciak V, Lobanov A, Lack J, Cam M, Zheng Z-M. 2019.
1024 CRISPR/Cas9-Mediated Knockout and In Situ Inversion of the ORF57 Gene from All
1025 Copies of the Kaposi's Sarcoma-Associated Herpesvirus Genome in BCBL-1 Cells . J
1026 Virol https://doi.org/10.1128/jvi.00628-19.

1027 67. Sallah N, Palser AL, Watson SJ, Labo N, Asiki G, Marshall V, Newton R, Whitby D,
1028 Kellam P, Barroso I. 2018. Genome-wide sequence analysis of Kaposi sarcoma-associated
1029 herpesvirus shows diversification driven by recombination. J Infect Dis
1030 https://doi.org/10.1093/infdis/jiy427.

1031 68. Tørresen OK, Star B, Mier P, Andrade-Navarro MA, Bateman A, Jarnot P, Gruca A,
1032 Grynberg M, Kajava A V., Promponas VJ, Anisimova M, Jakobsen KS, Linke D. 2019.
1033 Tandem repeats lead to sequence assembly errors and impose multi-level challenges for
1034 genome and protein databases. Nucleic Acids Res.

1035 69. Jain V, Plaisance-Bonstaff K, Sangani R, Lanier C, Dolce A, Hu J, Brulois K, Haecker I,
1036 Turner P, Renne R, Krueger B. 2016. A toolbox for Herpesvirus miRNA research:
1037 Construction of a complete set of KSHV miRNA Deletion Mutants. Viruses
1038 https://doi.org/10.3390/V8020054.

1039 70. Russo JJ, Bohenzky RA, Chien MC, Chen J, Yan M, Maddalena D, Parry JP, Peruzzi D,
1040 Edelman IS, Chang Y, Moore PS. 1996. Nucleotide sequence of the Kaposi sarcoma-
1041 associated herpesvirus (HHV8)Proceedings of the National Academy of Sciences of the
1042 United States of America.

1043 71. Dheekollu J, Chen H-S, Kaye KM, Lieberman PM. 2013. Timeless-Dependent DNA

1044 Replication-Coupled Recombination Promotes Kaposi's Sarcoma-Associated Herpesvirus
1045 Episome Maintenance and Terminal Repeat Stability. J Virol
1046 https://doi.org/10.1128/jvi.02211-12.

1047 72. Deutsch E, Cohen A, Kazimirsky G, Dovrat S, Rubinfeld H, Brodie C, Sarid R. 2004.
1048 Role of Protein Kinase C δ in Reactivation of Kaposi's Sarcoma-Associated Herpesvirus.
1049 J Virol https://doi.org/10.1128/jvi.78.18.10187-10192.2004.

1050 73. Miller G, Rigsby MO, Heston L, Grogan E, Sun R, Metroka C, Levy JA, Gao S-J, Chang
1051 Y, Moore P. 1996. Antibodies to Butyrate-Inducible Antigens of Kaposi's Sarcoma–
1052 Associated Herpesvirus in Patients with HIV-1 Infection. N Engl J Med
1053 https://doi.org/10.1056/nejm199605163342003.

1054 74. Chen J, Ueda K, Sakakibara S, Okuno T, Parravicini C, Corbellino M, Yamanishi K.
1055 2001. Activation of latent Kaposi's sarcoma-associated herpesvirus by demethylation of
1056 the promoter of the lytic transactivator. Proc Natl Acad Sci U S A
1057 https://doi.org/10.1073/pnas.051004198.

1058 75. Renne R, Zhong W, Herndier B, McGrath M, Abbey N, Kedes D, Ganem D. 1996. Lytic
1059 growth of Kaposi's sarcoma-associated herpesvirus (human herpesvirus 8) in culture. Nat
1060 Med https://doi.org/10.1038/nm0396-342.

1061 76. Ellison TJ, Kedes DH. 2014. Variable episomal silencing of a recombinant herpesvirus
1062 renders its encoded GFP an unreliable marker of infection in primary cells. PLoS One
1063 https://doi.org/10.1371/journal.pone.0111502.

1064 77. Haddad CO, Kalt I, Shovman Y, Xia L, Schlesinger Y, Sarid R, Parnas O. 2021. Targeting
1065 the Kaposi's sarcoma-associated herpesvirus genome with the CRISPR-Cas9 platform in

1066 latently infected cells. Virol J https://doi.org/10.1186/s12985-021-01527-x.

1067 78. Wen J, Zhao S, He D, Yang Y, Li Y, Zhu S. 2012. Preparation and characterization of egg
1068 yolk immunoglobulin Y specific to influenza B virus. Antiviral Res
1069 https://doi.org/10.1016/j.antiviral.2011.11.005.

1070 79. Brulois K, Toth Z, Wong L-Y, Feng P, Gao S-J, Ensser A, Jung JU. 2014. Kaposi's
1071 Sarcoma-Associated Herpesvirus K3 and K5 Ubiquitin E3 Ligases Have Stage-Specific
1072 Immune Evasion Roles during Lytic Replication. J Virol
1073 https://doi.org/10.1128/jvi.00873-14.

1074 80. Butnaru M, Gaglia MM. 2019. The kaposi's sarcoma-associated herpesvirus protein orf42
1075 is required for efficient virion production and expression of viral proteins. Viruses
1076 https://doi.org/10.3390/v11080711.

1077 81. Jiang HY, Yang WH, Gulick T, Bloch KD, Bloch DB. 2005. Ge-1 is a central component
1078 of the mammalian cytoplasmic mRNA processing body. RNA
1079 https://doi.org/10.1261/rna.2142405.

1080 82. Standart N, Weil D. 2018. P-Bodies: Cytosolic Droplets for Coordinated mRNA Storage.
1081 Trends Genet.

1082 83. Tenekeci U, Poppe M, Beuerlein K, Buro C, Müller H, Weiser H, Kettner-Buhrow D,
1083 Porada K, Newel D, Xu M, Chen ZJ, Busch J, Schmitz ML, Kracht M. 2016. K63-
1084 Ubiquitylation and TRAF6 Pathways Regulate Mammalian P-Body Formation and
1085 mRNA Decapping. Mol Cell https://doi.org/10.1016/j.molcel.2016.05.017.

1086 84. Seto E, Yoshida-Sugitani R, Kobayashi T, Toyama-Sorimachi N. 2015. The assembly of

1087 EDC4 and Dcp1a into processing bodies is critical for the translational regulation of IL-6.
1088 PLoS One https://doi.org/10.1371/journal.pone.0123223.

1089 85. Robinson C-A, Singh GK, Castle EL, Boudreau BQ, Corcoran JA. 2021. The
1090 NDP52/CALCOCO2 selective autophagy receptor controls processing body disassembly.
1091 bioRxiv.

1092 86. Ciufo DM, Cannon JS, Poole LJ, Wu FY, Murray P, Ambinder RF, Hayward GS. 2001.
1093 Spindle Cell Conversion by Kaposi's Sarcoma-Associated Herpesvirus: Formation of
1094 Colonies and Plaques with Mixed Lytic and Latent Gene Expression in Infected Primary
1095 Dermal Microvascular Endothelial Cell Cultures. J Virol
1096 https://doi.org/10.1128/jvi.75.12.5614-5626.2001.

1097 87. Grossmann C, Podgrabinska S, Skobe M, Ganem D. 2006. Activation of NF-κB by the
1098 Latent vFLIP Gene of Kaposi's Sarcoma-Associated Herpesvirus Is Required for the
1099 Spindle Shape of Virus-Infected Endothelial Cells and Contributes to Their
1100 Proinflammatory Phenotype. J Virol https://doi.org/10.1128/jvi.01603-05.

1101 88. Alkharsah KR, Singh V V., Bosco R, Santag S, Grundhoff A, Konrad A, Sturzl M, Wirth
1102 D, Dittrich-Breiholz O, Kracht M, Schulz TF. 2011. Deletion of Kaposi's Sarcoma-
1103 Associated Herpesvirus FLICE Inhibitory Protein, vFLIP, from the Viral Genome
1104 Compromises the Activation of STAT1-Responsive Cellular Genes and Spindle Cell
1105 Formation in Endothelial Cells. J Virol https://doi.org/10.1128/jvi.00226-11.

1106 89. Yoo J, Kang J, Lee HN, Aguilar B, Kafka D, Lee S, Choi I, Lee J, Ramu S, Haas J, Koh
1107 CJ, Hong YK. 2010. Kaposin-B enhances the PROX1 mRNA stability during lymphatic
1108 reprogramming of vascular endothelial cells by Kaposi's sarcoma herpes virus. PLoS

1109 Pathog https://doi.org/10.1371/journal.ppat.1001046.

1110 90. Chang HC, Hsieh TH, Lee YW, Tsai CF, Tsai YN, Cheng CC, Wang HW. 2016. c-Myc
1111 and viral cofactor Kaposin B co-operate to elicit angiogenesis through modulating
1112 miRNome traits of endothelial cells. BMC Syst Biol https://doi.org/10.1186/s12918-015-
1113 0242-3.

1114 91. Aguilar B, Choi I, Choi D, Chung HK, Lee S, Yoo J, Lee YS, Maeng YS, Lee HN, Park
1115 E, Kim KE, Kim NY, Baik JM, Jung JU, Koh CJ, Hong YK. 2012. Lymphatic
1116 reprogramming by Kaposi sarcoma herpes virus promotes the oncogenic activity of the
1117 virus-encoded G-protein-coupled receptor. Cancer Res https://doi.org/10.1158/0008-
1118 5472.CAN-12-1229.

1119 92. Toth Z, Papp B, Brulois K, Choi YJ, Gao SJ, Jung JU. 2016. LANA-Mediated
1120 Recruitment of Host Polycomb Repressive Complexes onto the KSHV Genome during De
1121 Novo Infection. PLoS Pathog https://doi.org/10.1371/journal.ppat.1005878.

1122 93. Gallo A, Lampe M, Günther T, Brune W. 2017. The Viral Bcl-2 Homologs of Kaposi's
1123 Sarcoma-Associated Herpesvirus and Rhesus Rhadinovirus Share an Essential Role for
1124 Viral Replication. J Virol https://doi.org/10.1128/jvi.01875-16.

1125 94. Campbell M, Watanabe T, Nakano K, Davis RR, Lyu Y, Tepper CG, Durbin-Johnson B,
1126 Fujimuro M, Izumiya Y. 2018. KSHV episomes reveal dynamic chromatin loop formation
1127 with domain-specific gene regulation. Nat Commun https://doi.org/10.1038/s41467-017-
1128 02089-9.

1129 95. West JA, Wicks M, Gregory SM, Chugh P, Jacobs SR, Zhang Z, Host KM, Dittmer DP,
1130 Damania B. 2014. An Important Role for Mitochondrial Antiviral Signaling Protein in the

1131 Kaposi's Sarcoma-Associated Herpesvirus Life Cycle. J Virol
1132 https://doi.org/10.1128/jvi.03226-13.

1133 96. Barbera AJ, Chodaparambil J V., Kelley-Clarke B, Joukov V, Walter JC, Luger K, Kaye
1134 KM. 2006. The nucleosomal surface as a docking station for Kaposi's sarcoma
1135 herpesvirus LANA. Science (80-) https://doi.org/10.1126/science.1120541.

1136 97. Hellert J, Weidner-Glunde M, Krausze J, Richter U, Adler H, Fedorov R, Pietrek M,
1137 Rückert J, Ritter C, Schulz TF, Lührs T. 2013. A Structural Basis for BRD2/4-Mediated
1138 Host Chromatin Interaction and Oligomer Assembly of Kaposi Sarcoma-Associated
1139 Herpesvirus and Murine Gammaherpesvirus LANA Proteins. PLoS Pathog
1140 https://doi.org/10.1371/journal.ppat.1003640.

1141 98. Vladimirova O, de Leo A, Deng Z, Wiedmer A, Hayden J, Lieberman PM. 2021. Phase
1142 separation and DAXX redistribution contribute to LANA nuclear body and KSHV
1143 genome dynamics during latency and reactivation. PLoS Pathog
1144 https://doi.org/10.1371/journal.ppat.1009231.

1145 99. Lin CL, Li H, Wang Y, Zhu FX, Kudchodkar S, Yuan Y. 2003. Kaposi's Sarcoma-
1146 Associated Herpesvirus Lytic Origin (ori-Lyt)-Dependent DNA Replication: Identification
1147 of the ori-Lyt and Association of K8 bZip Protein with the Origin. J Virol
1148 https://doi.org/10.1128/jvi.77.10.5578-5588.2003.

1149 100. Wang Y, Li H, Chan MY, Zhu FX, Lukac DM, Yuan Y. 2004. Kaposi's Sarcoma-
1150 Associated Herpesvirus ori-Lyt-Dependent DNA Replication: cis-Acting Requirements
1151 for Replication and ori-Lyt-Associated RNA Transcription. J Virol
1152 https://doi.org/10.1128/jvi.78.16.8615-8629.2004.

1153 101. Wang Y, Tang Q, Maul GG, Yuan Y. 2006. Kaposi's Sarcoma-Associated Herpesvirus
1154 ori-Lyt-Dependent DNA Replication: DualRole of Replication and Transcription
1155 Activator. J Virol https://doi.org/10.1128/jvi.00990-06.

1156 102. Liu D, Wang Y, Yuan Y. 2018. Kaposi's Sarcoma-Associated Herpesvirus K8 Is an RNA
1157 Binding Protein That Regulates Viral DNA Replication in Coordination with a Noncoding
1158 RNA. J Virol https://doi.org/10.1128/jvi.02177-17.

1159 103. Sharma NR, Majerciak V, Kruhlak MJ, Yu L, Kang JG, Yang A, Gu S, Fritzler MJ, Zheng
1160 ZM. 2019. KSHV RNA-binding protein ORF57 inhibits P-body formation to promote
1161 viral multiplication by interaction with Ago2 and GW182. Nucleic Acids Res
1162 https://doi.org/10.1093/nar/gkz683.

1163 104. Wang X, Chang L, Wang H, Su A, Wu Z. 2017. Dcp1a and GW182 Induce Distinct
1164 Cellular Aggregates and Have Different Effects on microRNA Pathway. DNA Cell Biol
1165 https://doi.org/10.1089/dna.2017.3633.

1166 105. Johnston BP, Pringle ES, McCormick C. 2019. KSHV activates unfolded protein response
1167 sensors but suppresses downstream transcriptional responses to support lytic replication.
1168 PLoS Pathog https://doi.org/10.1371/journal.ppat.1008185.

1169

1170

1171 **Table 1: BAC16 Mutagenesis Primers**

Primer *Fwd. is forward primer* *Rev. is reverse primer*	**Sequence** *Restriction enzyme recognition sites are bolded* *BAC16 homology regions are underlined* *Complementary target sequences are italicized.*
KanSacB Homology – Fwd.	5' ATACAT**GGATCC***AGGATGACGACGATAA GTAGGGATAACAGGGTAAT* 3'
KanSacB Homology – Rev.	5' ATTAGT**GCGGCCGC**GGACATGAACTGCC ACAAACACCGTTAAGCCTCTATCCAT*CAACCAAT TAACCAATTCTGAT* 3'
altKapC Homology – Fwd.	5' ATACAT**GCTAGC**CGGAGGACGGATCTCT TGGATTTACACGTATCGAGGAGCG*GTAGCACCC CAGGAACCCGTCCTAGCACACCCCA* 3'
altKapC Homology – Rev.	5' TGATTA**GGATCC**GGACATGAACTGCCAC AAACACCGTTAAGCCTCTATCCATA*CACTGAGAT TGAAGAG* 3'
altKapB Homology – Fwd.	5' ATACAT**GCTAGC**CGGAGGACGGATCTCT TGGATTTACACGTATCGAGGAGCG*GTGGCACCC CAGGAACCCGT* 3'
altKapB Homology – Rev.	5' TGATTA**GGATCC**GGACATGAACTGCCAC AAACACCGTTAAGCCTCTATCCAT*GCATAGGTAT AGGTGGTAGA* 3'
Kaposin Screening – Fwd.	5' *CAGGAAACGCTATAAAGAAGAGG* 3'

Kaposin Screening – Rev.	5’ *ACAGACAAACGAGTGGTGGTATC* 3’
altKapC Screening – Rev.	5’ *ATTACCTGGAAGCAATGCACC* 3’
altKapB Screening – Rev.	5’ *TGATGAAGGAACTAGATTGCCAG* 3’
KanSacB Screening – Fwd.	5’ *GCGACAACCATACGCTGAGAG* 3’
Revertant Screening – Rev. (Homology primer)	5’ *ACACCGTTAAGCCTCTATCCAT* 3’
Revertant Screening – Rev. (Revert primer)	5’ *TGCATTGGGATTGGAGTGAGGA* 3’

1172

1173

1174

1175

1176

1177

1178

1179

1180

1181

1182

1183

1184

1185 **Table 2: Antibodies**

Antibody	Species	Vendor/Catalogue #	Application	Dilution
Hedls	Mouse	Santa-Cruz sc-8418	Immunofluorescence	1:1000
KapB	Rabbit	A generous gift from Don Ganem	Immunoblot	1:1000
LANA	Rabbit	A generous gift from Don Ganem	Immunofluorescence Immunoblot	1:1000 1:1000
Alexa Fluor™ 647 Phalloidin	N/A	Thermo Fisher A22287	Immunofluorescence	1:100
Alexa Fluor™ 488	Chicken anti-Rabbit	Thermo Fisher A-21441	Immunofluorescence	1:1000
Alexa Fluor™ 647	Chicken anti-Mouse	Thermo Fisher A-21463	Immunofluorescence	1:1000
Hoechst 33342	N/A	Thermo Fisher H3570	Immunofluorescence	1:10000
Beta-Actin HRP Conjugate	Rabbit	Cell Signaling Technologies 5125	Immunoblot	1:8000
Anti-rabbit IgG HRP-linked	N/A	Cell Signaling Technologies 7074	Immunoblot	1:3000

1186

1187

1188

1189

1190

1191

1192 **Table 3: qPCR primers**

Primer	Sequence
ORF26 – Forward	5’ CAGTTGAGCGTCCCAGATGA 3’
ORF26 – Reverse	5’ GGAATACCAACAGGAGGCCG 3’
β-actin – Forward	5’ CTTCCAGCAGATGTGGATCA 3’
β-actin – Reverse	5’ AAAGCCATGCCAATCTCATC 3’
Luc – Forward	5’ TGCGCAAGAATAGCTCCTCC 3’
Luc – Reverse	5’ TTCGGCAACCAGATCATCCC 3’
IL-6 – Forward	5’ GTCCAGTTGCCTTCTCCCTGG 3’
IL-6 – Reverse	5’ GAGATGCCGTCGAGGATGTACC 3’
CSF2 – Forward	5’ AAATGTTTGACCTCCAGGAGCC 3’
CSF2 - Reverse	5’ ATCTGGGTTGCACAGGAAGTT 3’
VEGFA – Forward	5’ CGAGACCTTGGTGGACATC 3’
VEGFA – Reverse	5’ CTGCATGGTGACGTTGAAC 3’
IL-1β – Forward	5’ CTCTCACCTCTCCTACTCACTT 3’
IL-1β – Reverse	5’ TCAGAATGTGGGAGCGAATG 3’
LANA – Forward	5’ GCGAAGGAAGCATGTCGCC 3’
LANA – Reverse	5’ CACAGGATGGGATGGAGGGATTG 3’
18S – Forward	5’ CGTTCTTAGTTGGTGGAGCG 3’
18S – Reverse	5’ CCGGACATCTAAGGGCATCA 3’
HPRT-1 – Forward	5’ TGGCGTCGTGATTAGTGATG 3’
HPRT-1 – Reverse	5’ GACGTTCAGTCCTGTCCATAAT 3’

1193

1194

1195

1196

1197 **Table 4: Plasmids**

Plasmid	Use	Source	Mammalian Selection
pcDNA3.1 (+)	Empty Vector Control	Invitrogen V79020	N/A
pcDNA3.1 KapB KS lung	Overexpression	C. McCormick (Dalhousie University)	N/A
pcDNA3.1 KapB BAC16	Overexpression	Cloned from pUC57 KapB BAC16 (Bio Basic)	N/A
pLJM1	Empty Vector Control	(105)	Blasticidin
pLJM1 KapB (pulmonary KS)	Overexpression	Cloned from pBMNIP-KapB (51) into pLJM1-BSD	Blasticidin
pMD2.G	Lentivirus generation	Addgene #12259	N/A
psPAX2	Lentivirus generation	Addgene #12260	N/A

1198

1199

1200

1201

1202

1203

1204

1205 **<u>Figure Legends</u>**

1206 **Figure 1. Lambda Red recombination facilitates the creation of five kaposin-deficient**
1207 **BAC16 DNA constructs. (A)** A simplified version of the kaposin transcript is depicted in the 5'
1208 to 3' orientation. Open reading frames for kaposin A (KapA), kaposin B (KapB), and kaposin C
1209 (KapC) are indicated with corresponding AUG, GUG and CUG start codons for each. DR1 =
1210 direct repeat 1, DR2 = direct repeat 2, K12 = the KapA ORF. **(B)** An example of the re-coding
1211 strategy used to create the BAC16ΔKapB virus construct is shown. Wildtype nucleotide and
1212 corresponding amino acid repeats are show above with recoded nucleotides (red) and
1213 corresponding amino acid changes depicted below. **(C)** The Lambda Red recombination method
1214 used to create all kaposin-deficient BAC16 viruses is shown; the strategy for BAC16ΔKapB is
1215 depicted as an example. **(D)** Each kaposin-deficient BAC16 construct is shown relative to that of
1216 the wildtype *kaposin* locus in its genomic position (only reverse strand is shown for simplicity).

1217

1218 **Figure 2. Confirmation of the panel BAC16 kaposin-deficient viruses. (A)** BAC16 DNA was
1219 isolated from GS1783 *E.coli* harbouring recombinant or WT BAC16 DNA and then subjected to
1220 whole genome sequencing (WGS). Raw reads were paired, trimmed, and mapped to the BAC16
1221 genome (NCBI accession #GQ994935) in Geneious Prime. Coverage for each recombinant is
1222 indicated in blue with an average coverage per nucleotide of between 670-1430x. BAC16 ORFs
1223 are depicted in turquoise, repeat regions in orange and the *kaposin* locus is outlined in red.
1224 Variants were detected based on a minimum coverage of 5 and minimum frequency variation of
1225 0.25 and are depicted in magenta. **(B)** Representative zoom panels of read alignment to the
1226 *kaposin* locus of WT and ΔKapB are shown. **(C)** BAC16 DNA was isolated from GS1783 *E.coli*
1227 and digested using NheI and fragments were subjected to pulsed-field gel electrophoresis

1228 (PFGE). Based on *in silco* predictions, *kaposin* locus containing fragments are indicated with a
1229 red asterisk.

1230

1231 **Figure 3. Generation of stable latent kaposin-deficient BAC16 iSLK cell lines by co-culture**
1232 **method. (A-D)** 293T cells were transfected with recombinant or WT BAC16 DNA. 48 hours
1233 post transfection, cells were selected with hygromycin (increasing concentration from 50 µg/mL
1234 to 100 µg/mL) until a confluent layer of BAC16-containing 293T cells was achieved. **(B)** Images
1235 of BAC16-293Ts were captured using an EVOS-FL microscope with the 10X objective. **(C)**
1236 Latent BAC16-293T cells were trypsinzed, pelleted and lysed to extract DNA. qPCR was
1237 performed using ORF26 and β-actin specific primers. Values are represented as fold change
1238 relative WT. *n*=3; mean ± SD. **(D-F)** BAC16-293Ts were seeded in a 2:1 ratio with naïve iSLK
1239 cells. Cells were treated with 1 mM NaB and 20 ng/mL TPA for 96 hours, virus-containing
1240 supernatant was removed and replaced with media containing puromycin (10 µg/mL) and
1241 hygromycin (increasing concentration from 200 µg/mL to 1200 µg/mL) until a confluent layer of
1242 BAC16-containing iSLK cells was achieved **(E).** Latent iSLKs were fixed, permeabilized and
1243 immunostained using antisera for viral LANA (green) to visualize infected nuclei and Hoescht to
1244 visualize total cell nuclei (blue)**.** Images were captured using Zeiss AxioObserver Z1 microscope
1245 with the 40X objective. Scale bar = 20 µm. **(F)** BAC16-containing iSLKs were trypsinized,
1246 pelleted and lysed to extract DNA. qPCR was performed using ORF26 and β-actin specific
1247 primers. Values are represented as fold change relative to WT. *n*=3; mean ± SD, (*, $P < 0.05$; **,
1248 $P < 0.01$; ***, $P < 0.001$; ****, $P < 0.0001$; ns, nonsignificant).

1249

1250 **Figure 4. Removal of kaposin direct repeats accelerates KSHV episome loss from latent**
1251 **iSLK cells.** Latent iSLK cells were serially passaged in the absence of hygromycin for a total of
1252 14 passages. At each passage, a sample of cells was taken, pelleted and used for DNA extraction.
1253 To quantify levels of viral DNA, qPCR was performed using viral ORF26 and host β-actin
1254 specific primers. **(A)** Values are represented as fold change relative to genome copy number in
1255 wild-type (WT) BAC16 iSLK cells at passages 1 (P1) $n = 3$; means ± SD, (*, $P < 0.05$; **, $P <$
1256 0.01; ***, $P < 0.001$; ****, $P < 0.0001$; ns, nonsignificant). **(B)** Values are represented as fold
1257 change relative to the corresponding starting passage (P1), for each recombinant virus over the
1258 course of the experiment. $n = 3$; mean ± SD. The red line was obtained using linear regression
1259 analysis and the slope of the line is depicted in the top right corner for each graph.

1260

1261 **Figure 5. Kaposin-deficient BAC16 iSLK cells produce progeny virions when reactivated.**
1262 **(A)** BAC16-iSLK cells were reactivated using 1 μg/mL Dox for 24 hours prior to lysis and
1263 immunoblotting using antisera that recognizes DR1 in both KapB and KapC. Specific antibody
1264 to β-actin served as a loading control. One representative experiment of three is shown. **(B-C)**
1265 BAC16-iSLK cells were reactivated with 1 μg/mL Dox and 1 mM NaB for 0, 24, 48, 72, or 96
1266 hours. At each time point cells were trypsinized, pelleted and lysed to extract DNA. qPCR was
1267 performed using ORF26 and host β-actin specific primers. Values represent either fold-change
1268 relative to time 0 (latency) for each recombinant virus (B) n=3, mean ± SD, or fold-change
1269 relative to WT at 0, 24, 48, 72 and 96h post reactivation, (C) n=3; mean ± SD**,** (*, $P < 0.05$; **, P
1270 < 0.01; ***, $P < 0.001$; ****, $P < 0.0001$; ns, nonsignificant). **(D).** BAC16-iSLK cells were
1271 reactivated as above for 96h, virus-containing supernatant was collected, clarified and DNase-
1272 treated prior to extraction of virion-protected DNA. qPCR was performed using ORF26 and

1273 luciferase (control) specific primers. Values represented fold-change relative to WT. *n*=3; mean
1274 ± SD, (*, P < 0.05; **, P < 0.01; ***, P < 0.001; ****, P < 0.0001; ns, nonsignificant). **(E)**
1275 BAC16-iSLK cells were reactivated for 96 hours. Virus-containing supernatant for each
1276 recombinant cell line was then collected, clarified, and diluted 1:4 with fresh DMEM and used to
1277 infect naïve 293T cells. After 24h, cells were fixed, permeabilized and stained using antisera
1278 specific for viral LANA (green) and Hoescht (nucleus, blue)**.** Images were captured using Zeiss
1279 AxioObserver Z1 microscope with the 40X objective. Scale bar = 20 µm. One representative
1280 experiment is shown.

1281

1282 **Figure 6. Primary infection of endothelial cells with BAC16ΔKapB virus is impaired.**

1283 **(A-B)** Equal numbers of virus particles (based on DNase-protected extracellular genome copy
1284 number) of WT and either ΔKapB-1 and ΔKapB-2 were used to infect HUVECs. 24h later, cells
1285 were fixed, permeabilized and immunstained for viral LANA, then stained with Hoescht. The
1286 number of LANA-expressing cells was quantified and is represented as a percent of the total
1287 number of cells counted. *n*=2; mean ± SD. **(C)** Images of four different ΔKapB BAC16-iSLK
1288 latent cell lines and WT BAC16-iSLKs were captured using an EVOS-FL microscope with the
1289 10X objective. One representative experiment of two is shown. **(D-F)** Latent ΔKapB and WT
1290 BAC16-iSLKs were fixed, permeabilized and immunostained for viral LANA, then stained with
1291 Hoescht. LANA-NBs were visualized (D), and the number of LANA-NBs per cell was counted
1292 using CellProfiler (E) *n*=2; mean ± SD. LANA-NB area was calcuated for at approximently 4000
1293 individual LANA-NBs per cell line and the distribution of area shown in (F). **(G)** Latent ΔKapB
1294 and WT BAC16-iSLKs were trypsinized, pelleted and lysed to extract DNA. qPCR was
1295 performed using ORF26 and β-actin specific primers. Values are represented as fold change

1296 relative WT. *n*=3, mean ± SD**,** (*, P < 0.05; **, P < 0.01; ***, P < 0.001; ****, P < 0.0001; ns,
1297 nonsignificant). **(H)** Latent BAC16-iSLKs were lysed and harvested for immunoblotting using
1298 LANA and β-actin specific antibodies. One representative experiment of two is shown.

1299 **Figure 7. Ectopic expression of KapB does not rescue altered latency phenotypes in ΔKapB**
1300 **infected cells. (A-C)** Latent WT or ΔKapB BAC16-iSLK cells lines were transduced to express
1301 either an empty vector (EV) control or KapB (KS lung isolate). 24h later, cells were selected
1302 using blasticidin for 48h prior to seeding. The following day seeded cells were lysed and
1303 harvested for RNA or protein analysis. (A-B) RT-qPCR was performed using LANA and 18S
1304 specific primers. *n*=3; mean ± SD**,** (*, P < 0.05; **, P < 0.01; ***, P < 0.001; ****, P < 0.0001;
1305 ns, nonsignificant). In A, LANA RNA transcript levels in ΔKapB iSLK cell lines are shown
1306 normalized to WT iSLK cells. In B, LANA RNA transcript levels are shown after KapB
1307 complementation, normalized to each respective EV control. (C) Immunoblotting was
1308 performed using LANA, DR1 (KapB) and β-actin specific antibodies. One representative
1309 experiment of three is shown. **(D-F)** Naïve iSLK cells were transduced with EV or KapB
1310 lentiviruses as in (A). After seeding, cells were infected with equal particle numbers of WT and
1311 ΔKapB BAC16 viruses as determined via DNase-protected extracellular genome copy number.
1312 24h post infection, cells were either trypsinized, pelleted and lysed to extract DNA or lysed for
1313 immunoblotting. (D-E) qPCR was performed for KSHV DNA using ORF26 and host β-actin
1314 specific primers. *n*=3; mean ± SD**,** (*, P < 0.05; **, P < 0.01; ***, P < 0.001; ****, P < 0.0001;
1315 ns, nonsignificant). In D, Viral genome copy number for iSLKs after *de novo* infection with
1316 ΔKapB is normalized to the WT control. In E, viral genome copy number for each virus infection
1317 after complementing with KapB is normalized to each respective EV control. (F)
1318 Immunoblotting was performed using LANA, DR1 (KapB) and β-actin specific antibodies. One

1319 representative experiment of three is shown. **(G-I)** 293T cells were transfected with three
1320 different ectopic expression constructs for KapB: KapB derived from KS lung (45) and KapB
1321 BAC16. 24 h after transfection, cells were infected with equal particle numbers of WT and
1322 ΔKapB BAC16 viruses and processed as above for qPCR (G-H, *n*=3; mean ± SD**,** (*, P < 0.05;
1323 **, P < 0.01; ***, P < 0.001; ****, P < 0.0001; ns, nonsignificant). or immunoblotting (I, n=1).
1324 In G, Viral genome copy number for 293Ts after *de novo* infection with ΔKapB is normalized to
1325 the WT control. In H, viral genome copy number for each virus infection after complementing
1326 with different versions of KapB is normalized to each respective EV control.

1327 **Figure 8. KapB is required for PB disassembly following *de novo* HUVEC infection. (A)**
1328 WT and ΔKapB BAC16 viruses were titrated using 293T cells and RFP expression was used to
1329 estimate an equal number of infectious virions for subsequent *de novo* infection of HUVECs. At
1330 96hpi, HUVECs were fixed, permeabilized and immunostained for either viral LANA (green),
1331 the PB-resident protein Hedls/EDC4 (white) then stained with Hoescht (nucleus, blue). Images
1332 were captured using Zeiss AxioObserver Z1 microscope with the 40X objective. Scale bar = 20
1333 μm. **(B)** Hedls puncta per cell were quantified using CellProfiler. For mock infections, all cells
1334 were counted; for WT and ΔKapB-infected cells, only LANA-positive cells were counted. Data
1335 is represented as fold change in PBs per cell relative to mock infection. *n*=4; mean ± SD, (*, P <
1336 0.05; **, P < 0.01; ***, P < 0.001; ****, P < 0.0001; ns, nonsignificant). **(C)** Cells infected as in
1337 (A) were lysed at 96 hpi and harvested for immunoblotting using LANA, DR1 (KapB and C) and
1338 β-actin specific antibodies. One representative experiment of three is shown. **(D)** Cells infected
1339 as in (A) were lysed at 96 and 120 hpi and harvested for RNA extraction and RT-qPCR using IL-
1340 6, CSF2, VEGFA, IL-1β and HPRT specific primers. *n*=3; mean ± SD**,** (*, P < 0.05; **, P <
1341 0.01; ***, P < 0.001; ****, P < 0.0001; ns, nonsignificant).

1342 **Figure 9 KapB is not required for endothelial cell spindling following de novo HUVEC**
1343 **infection.** WT and ΔKapB BAC16 viruses were titrated using 293T cells and RFP expression
1344 was used to estimate an equal number of infectious virions for subsequent *de novo* infection of
1345 HUVECs, as in Figure 8. At 96 hpi, brightfield images were acquired at 10X, cells were fixed,
1346 permeabilized and immunostained for viral LANA (green). Phalloidin and Hoescht staining was
1347 used to visualize actin (white) and nuclei (blue), respectively. Images were captured using Zeiss
1348 AxioObserver Z1 microscope with the 40X objective. Scale bar = 20 μm. One representative
1349 image of three experiments is shown.

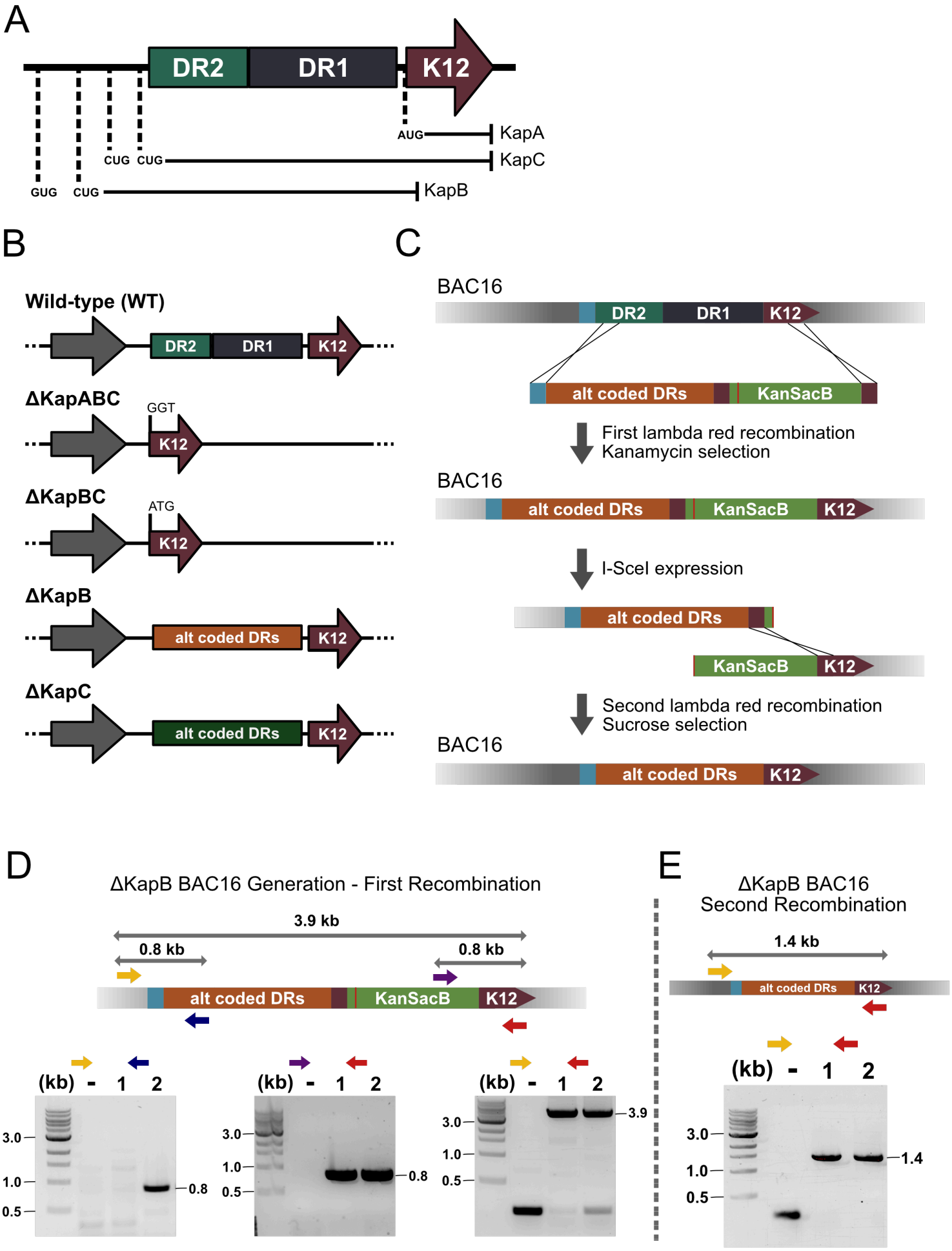
A
DR2
DR1
K12
AUG
KapA
CUG CUG
KapC
GUG CUG
KapB
B
Wild-type (WT)
DR2
DR1
K12
ΔKapABC
GGT
K12
ΔKapBC
ATG
K12
ΔKapB
alt coded DRs
K12
ΔKapC
alt coded DRs
K12
C
BAC16
DR2
DR1
K12
alt coded DRs
KanSacB
First lambda red recombination
Kanamycin selection
BAC16
alt coded DRs
KanSacB
K12
I-SceI expression
alt coded DRs
KanSacB
K12
Second lambda red recombination
Sucrose selection
BAC16
alt coded DRs
K12
D
ΔKapB BAC16 Generation - First Recombination
3.9 kb
0.8 kb
0.8 kb
alt coded DRs
KanSacB
K12
(kb) - 1 2
3.0
1.0
0.5
0.8
(kb) - 1 2
3.0
1.0
0.5
0.8
(kb) - 1 2
3.0
1.0
0.5
3.9
E
ΔKapB BAC16
Second Recombination
1.4 kb
alt coded DRs
K12
(kb) - 1 2
3.0
1.0
0.5
1.4

A

Wild-type BAC16

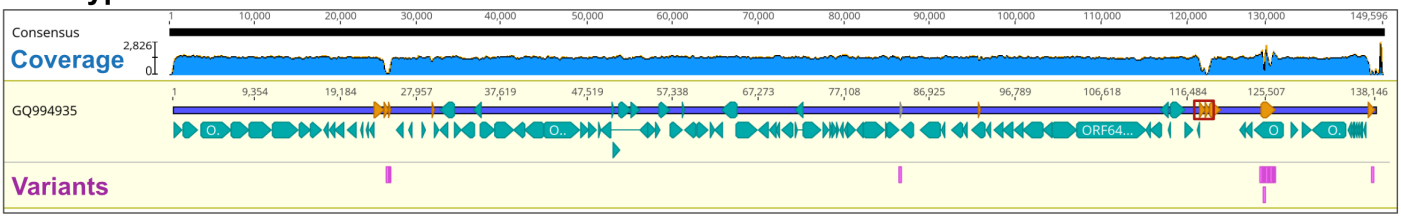

BAC16ΔKapABC

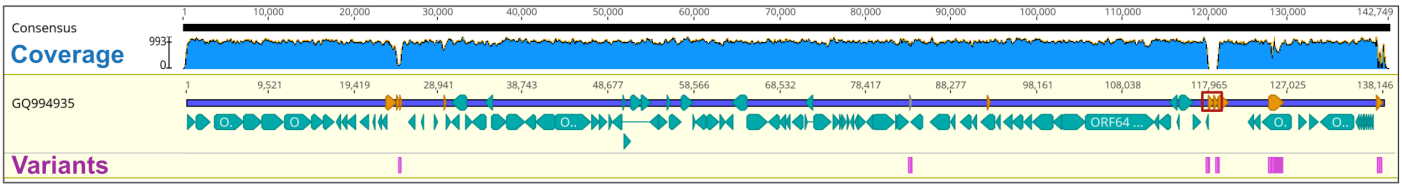

BAC16ΔKapBC

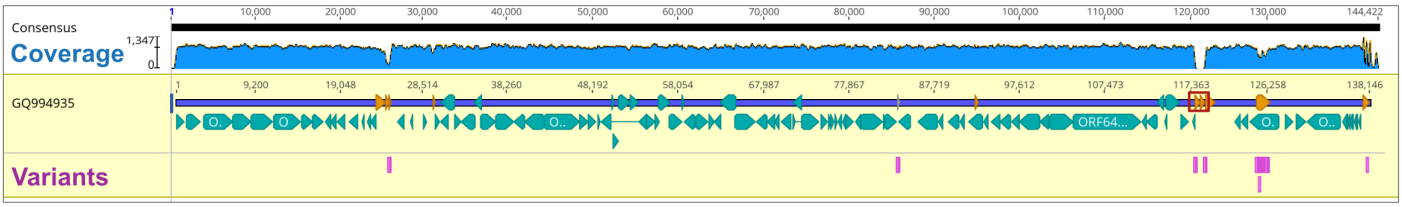

BAC16ΔKapB

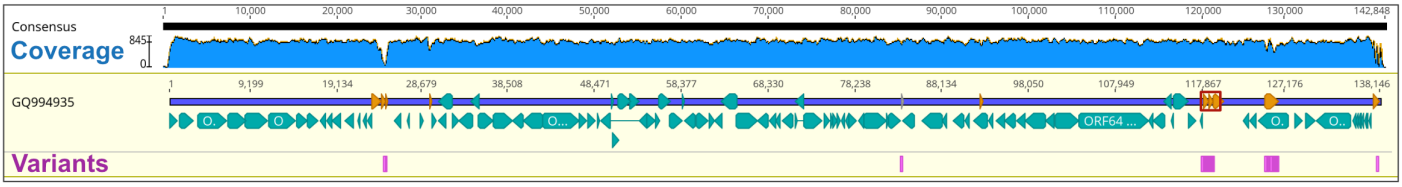

BAC16ΔKapC

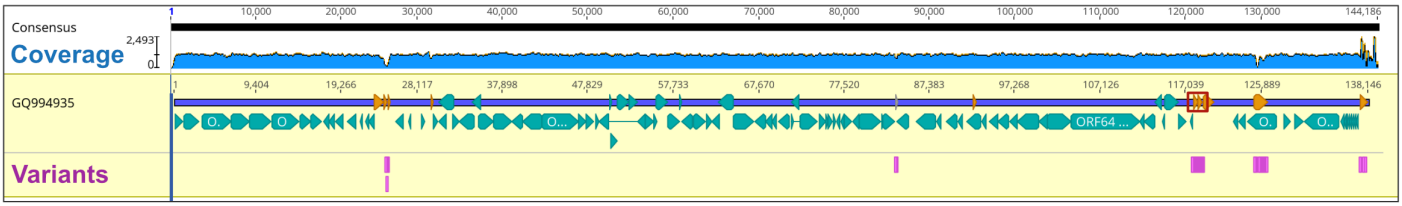

B

Wild-type kaposin

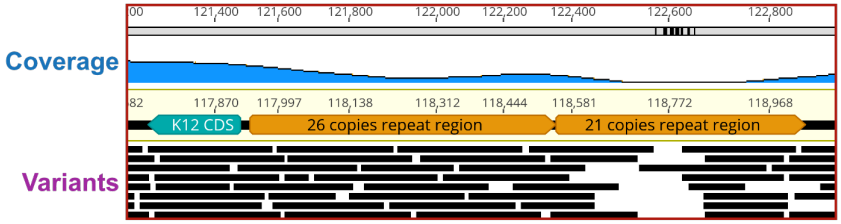

BAC16ΔKapB kaposin

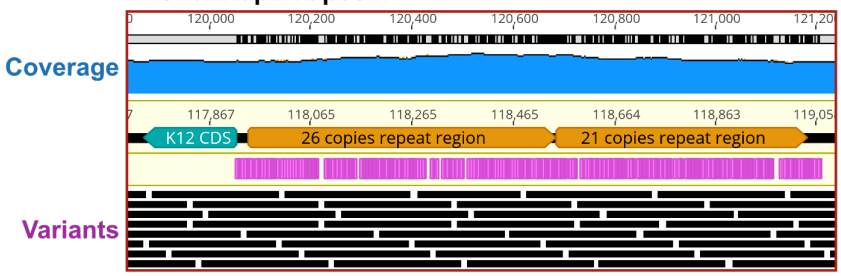

C

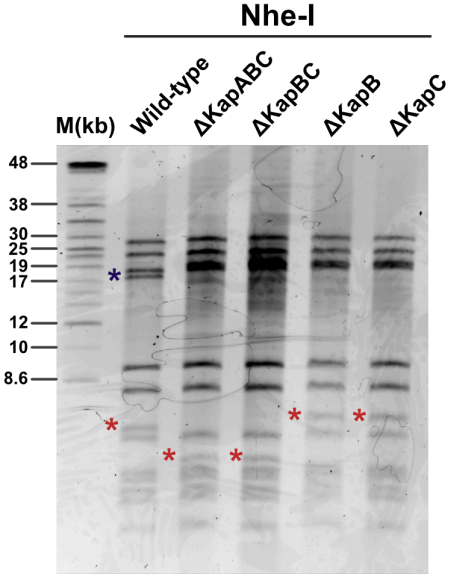

A

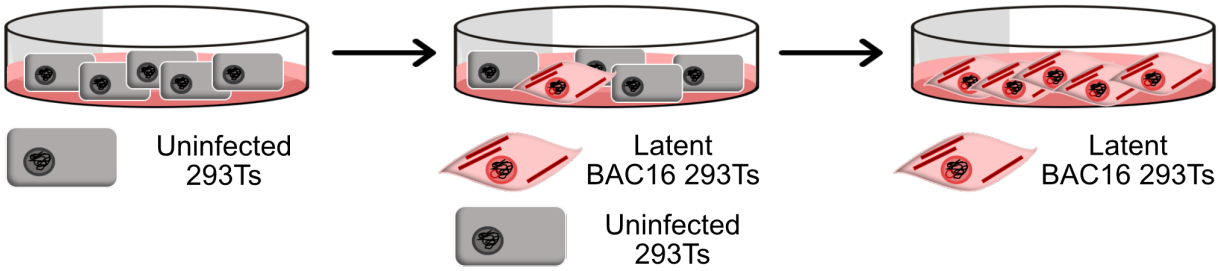
Transfection:
BAC16 DNA
Selection:
Hygromycin
Uninfected
293Ts
Latent
BAC16 293Ts
Uninfected
293Ts
Latent
BAC16 293Ts

B

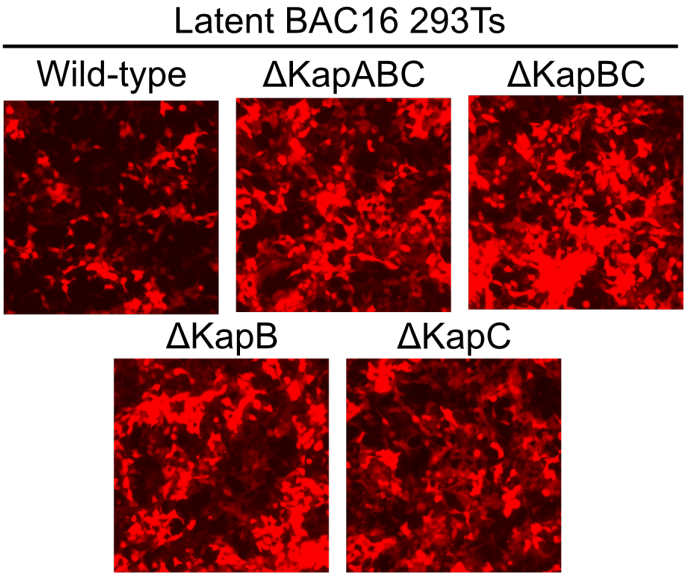
Latent BAC16 293Ts
Wild-type
ΔKapABC
ΔKapBC
ΔKapB
ΔKapC

C

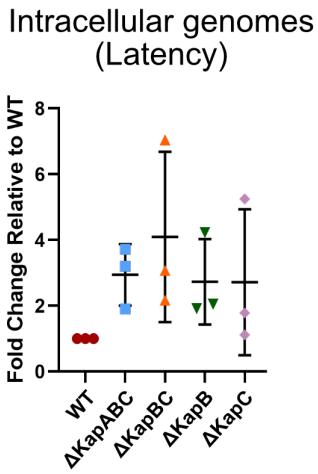
Intracellular genomes
(Latency)
Fold Change Relative to WT
0
2
4
6
8
WT
ΔKapABC
ΔKapBC
ΔKapB
ΔKapC

D

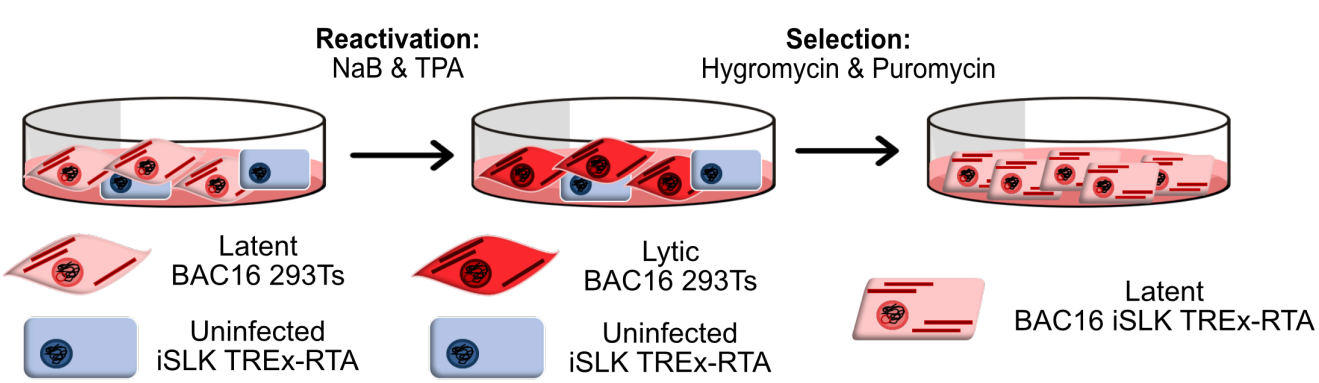
Reactivation:
NaB & TPA
Selection:
Hygromycin & Puromycin
Latent
BAC16 293Ts
Uninfected
iSLK TREx-RTA
Lytic
BAC16 293Ts
Uninfected
iSLK TREx-RTA
Latent
BAC16 iSLK TREx-RTA

E

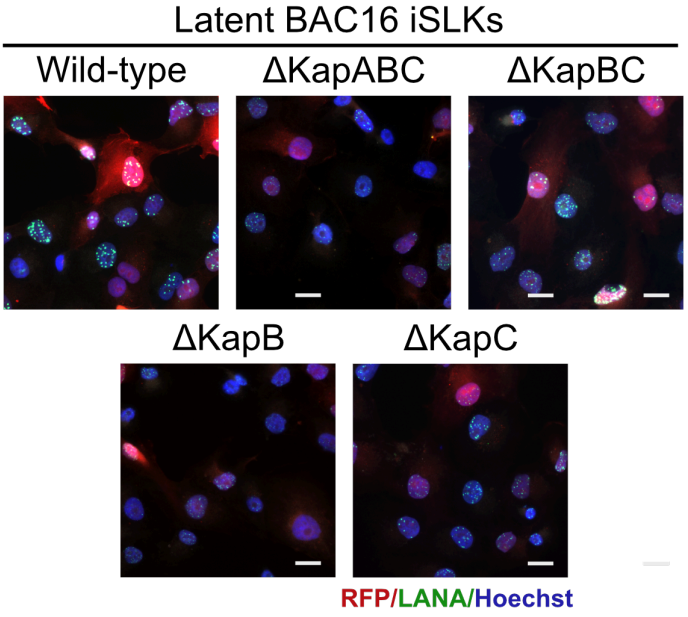
Latent BAC16 iSLKs
Wild-type
ΔKapABC
ΔKapBC
ΔKapB
ΔKapC
RFP/LANA/Hoechst

F

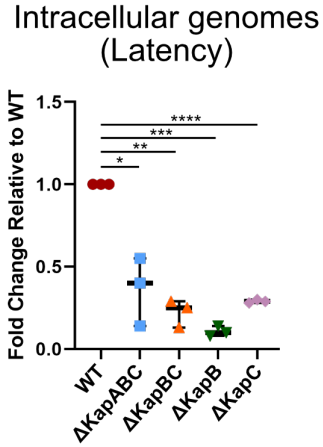
Intracellular genomes
(Latency)
Fold Change Relative to WT
0.0
0.5
1.0
1.5
*
**
***
****
WT
ΔKapABC
ΔKapBC
ΔKapB
ΔKapC

A

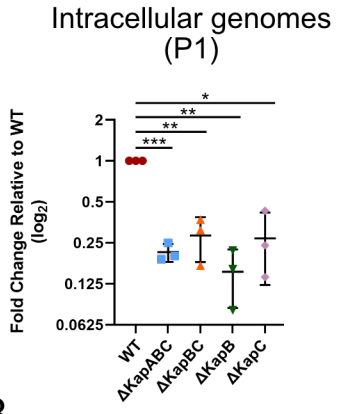
Intracellular genomes
(P1)
Fold Change Relative to WT
(log2)
2
1
0.5
0.25
0.125
0.0625
*
**
**
***
WT
ΔKapABC
ΔKapBC
ΔKapB
ΔKapC

B

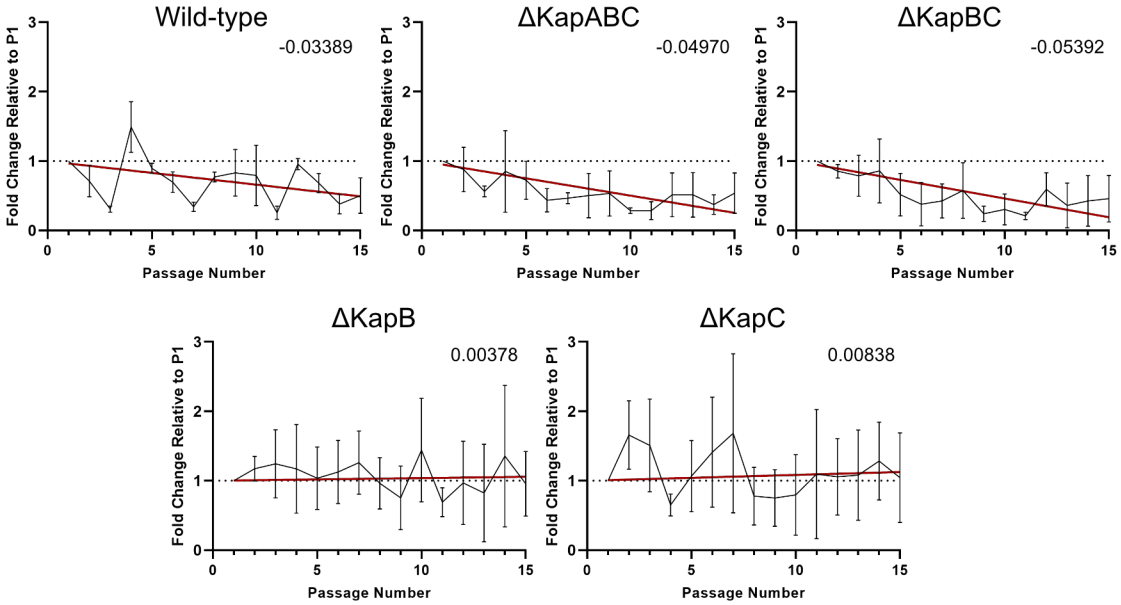
Wild-type
-0.03389
ΔKapABC
-0.04970
ΔKapBC
-0.05392
ΔKapB
0.00378
ΔKapC
0.00838
Fold Change Relative to P1
Passage Number
0
5
10
15
0
1
2
3

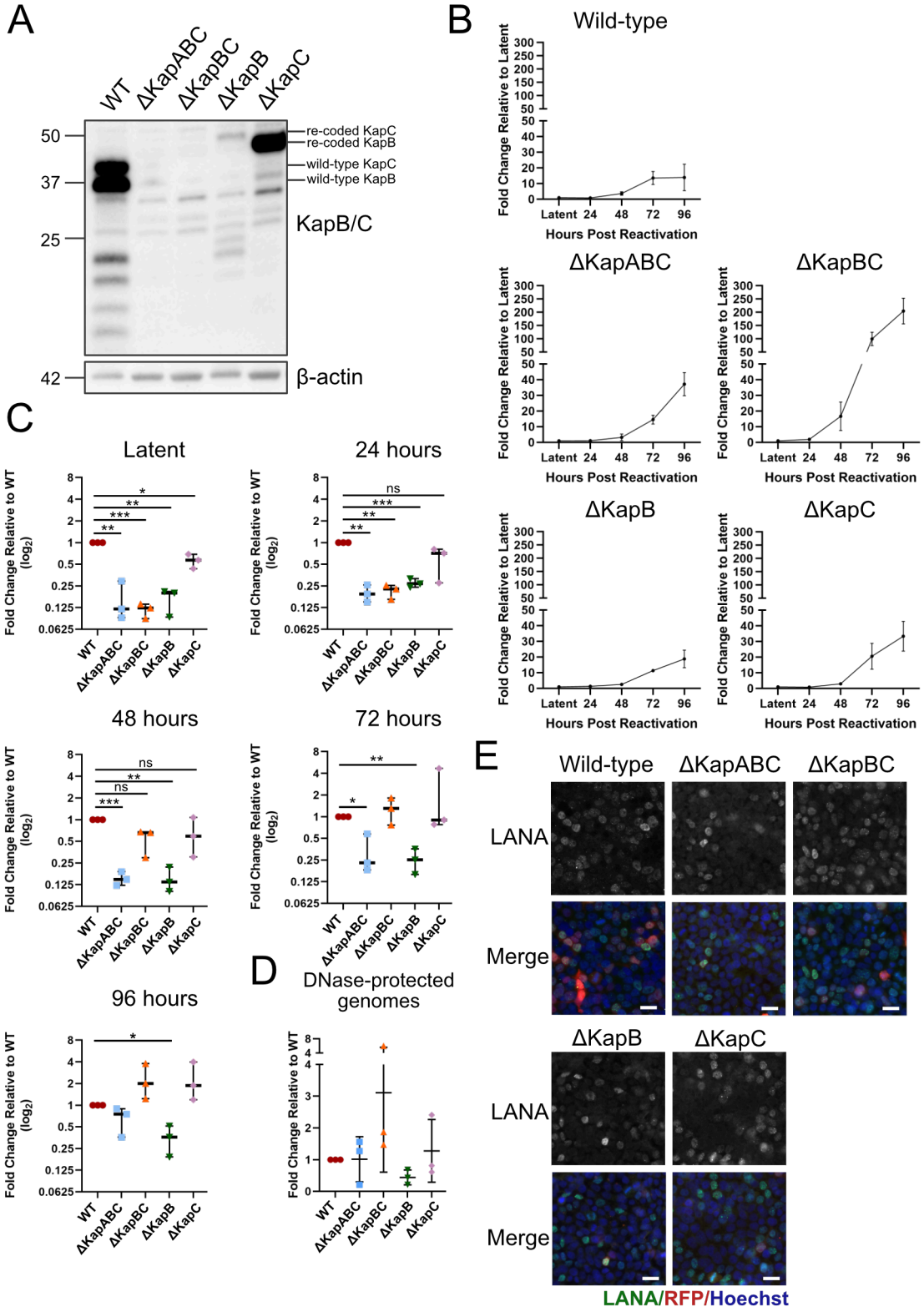
A
WT
ΔKapABC
ΔKapBC
ΔKapB
ΔKapC
50
37
25
42
re-coded KapC
re-coded KapB
wild-type KapC
wild-type KapB
KapB/C
β-actin
B
Wild-type
ΔKapABC
ΔKapBC
ΔKapB
ΔKapC
Fold Change Relative to Latent
Latent 24 48 72 96
Hours Post Reactivation
C
Latent
24 hours
48 hours
72 hours
96 hours
Fold Change Relative to WT (log2)
WT
ΔKapABC
ΔKapBC
ΔKapB
ΔKapC
D
DNase-protected genomes
E
Wild-type
ΔKapABC
ΔKapBC
ΔKapB
ΔKapC
LANA
Merge
LANA/RFP/Hoechst

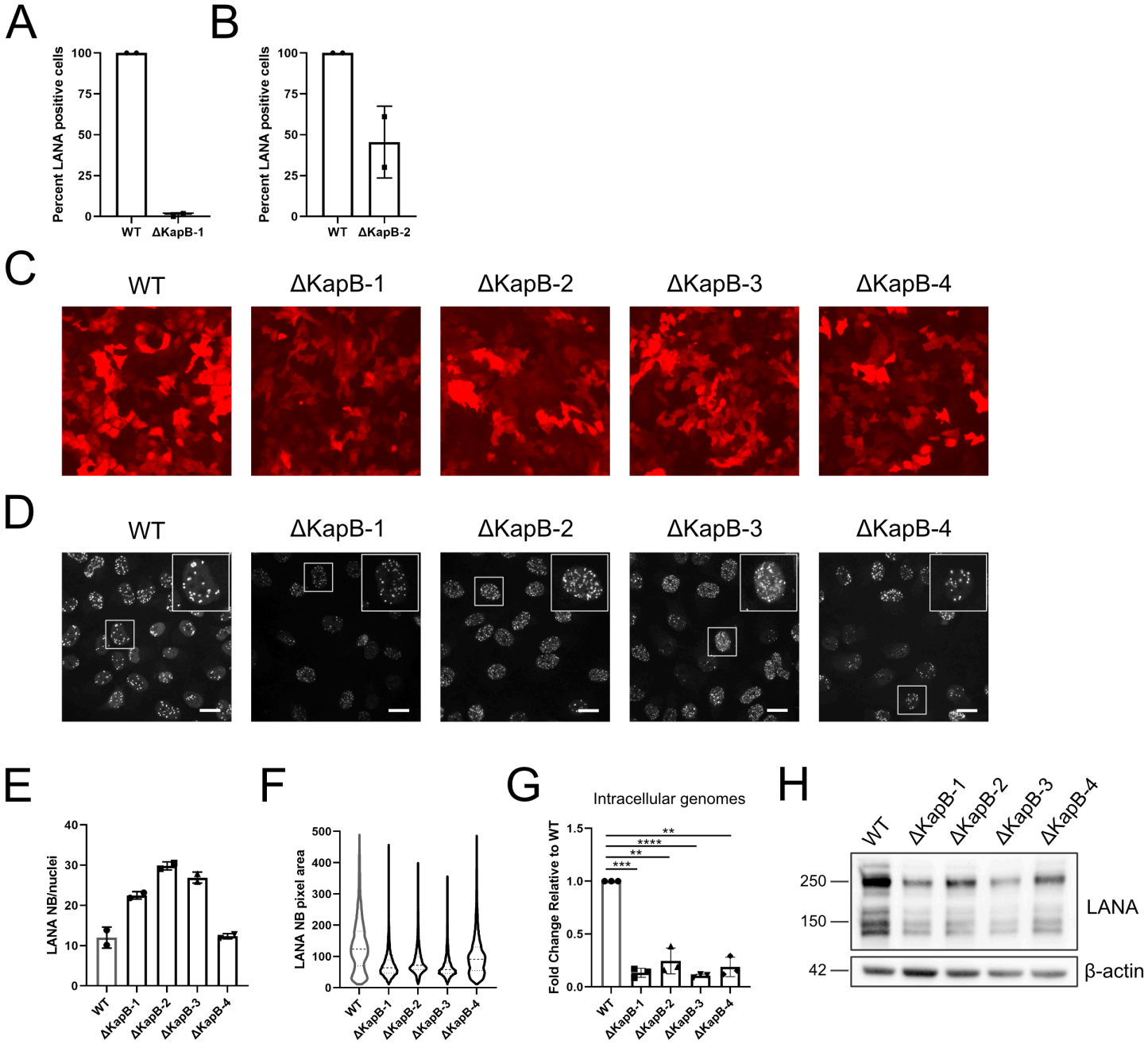
A
Percent LANA positive cells
100
75
50
25
0
WT
ΔKapB-1
B
Percent LANA positive cells
100
75
50
25
0
WT
ΔKapB-2
C
WT
ΔKapB-1
ΔKapB-2
ΔKapB-3
ΔKapB-4
D
WT
ΔKapB-1
ΔKapB-2
ΔKapB-3
ΔKapB-4
E
LANA NB/nuclei
40
30
20
10
0
WT
ΔKapB-1
ΔKapB-2
ΔKapB-3
ΔKapB-4
F
LANA NB pixel area
500
400
300
200
100
0
WT
ΔKapB-1
ΔKapB-2
ΔKapB-3
ΔKapB-4
G
Intracellular genomes
Fold Change Relative to WT
1.5
1.0
0.5
0.0
**
****
**
***
WT
ΔKapB-1
ΔKapB-2
ΔKapB-3
ΔKapB-4
H
WT
ΔKapB-1
ΔKapB-2
ΔKapB-3
ΔKapB-4
250
150
42
LANA
β-actin

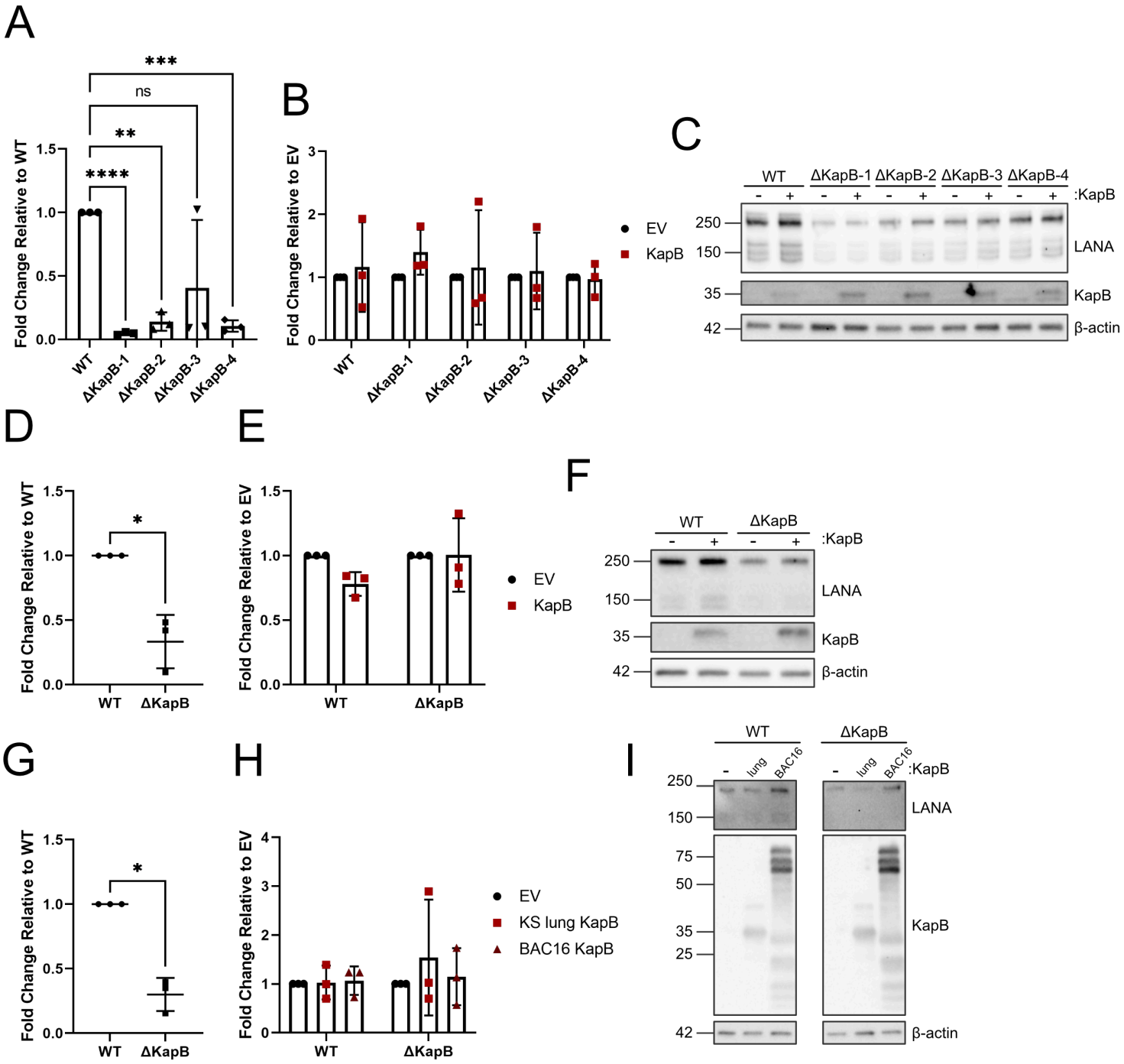
A
***
ns
**
****
Fold Change Relative to WT
1.5
1.0
0.5
0.0
WT
ΔKapB-1
ΔKapB-2
ΔKapB-3
ΔKapB-4
B
Fold Change Relative to EV
3
2
1
0
EV
KapB
C
WT
ΔKapB-1
ΔKapB-2
ΔKapB-3
ΔKapB-4
:KapB
250
150
LANA
35
KapB
42
β-actin
D
Fold Change Relative to WT
*
WT
ΔKapB
E
Fold Change Relative to EV
EV
KapB
F
WT
ΔKapB
:KapB
250
150
LANA
35
KapB
42
β-actin
G
Fold Change Relative to WT
*
WT
ΔKapB
H
Fold Change Relative to EV
4
EV
KS lung KapB
BAC16 KapB
I
WT
ΔKapB
lung
BAC16
:KapB
250
150
LANA
75
50
35
25
KapB
42
β-actin

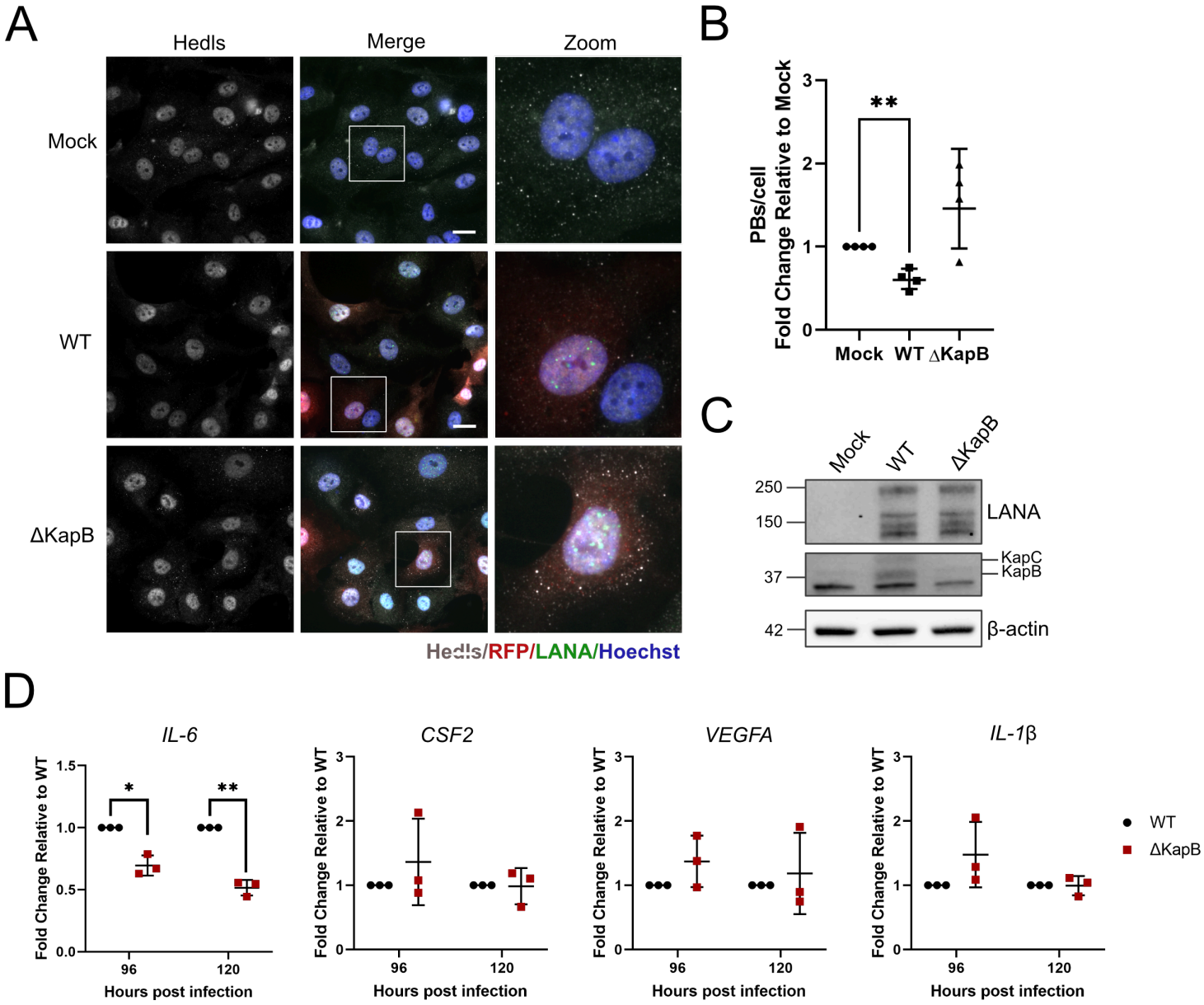
A
Hedls
Merge
Zoom
Mock
WT
ΔKapB
Hedls/RFP/LANA/Hoechst
B
PBs/cell
Fold Change Relative to Mock
**
Mock
WT
ΔKapB
C
Mock
WT
ΔKapB
250
150
37
42
LANA
KapC
KapB
β-actin
D
IL-6
CSF2
VEGFA
IL-1β
Fold Change Relative to WT
Hours post infection
96
120
*
**
WT
ΔKapB

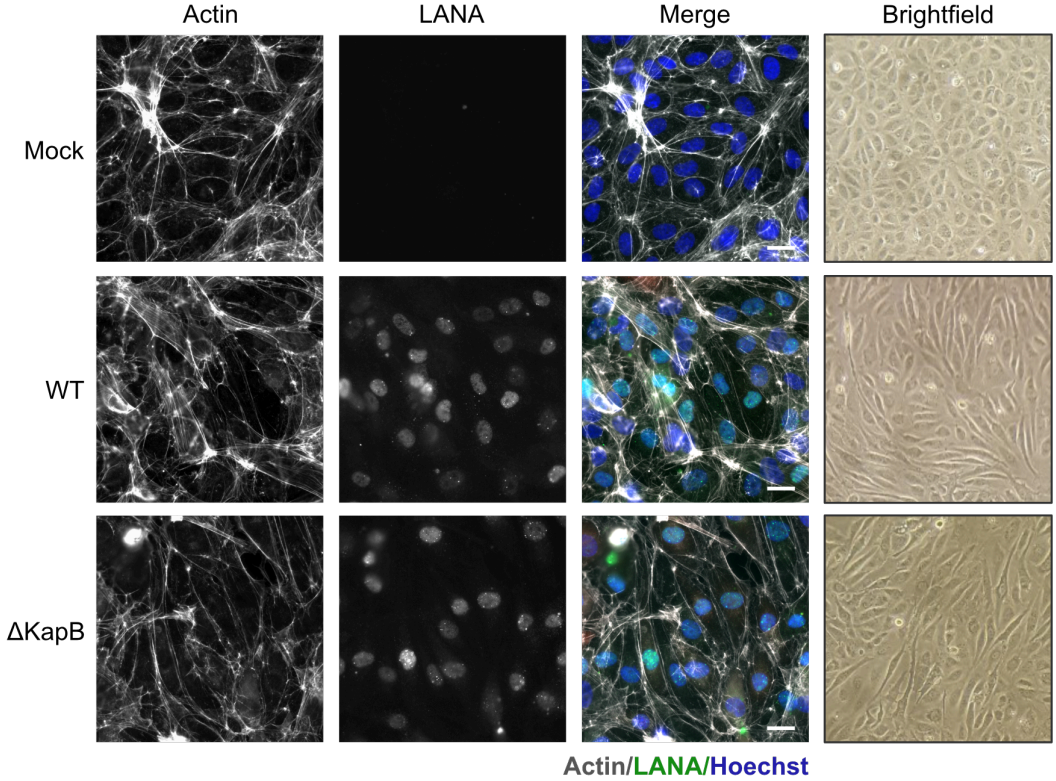
Actin
LANA
Merge
Brightfield
Mock
WT
ΔKapB
Actin/LANA/Hoechst